Charles University in Prague

Faculty of Mathematics and Physics

DIPLOMA THESIS

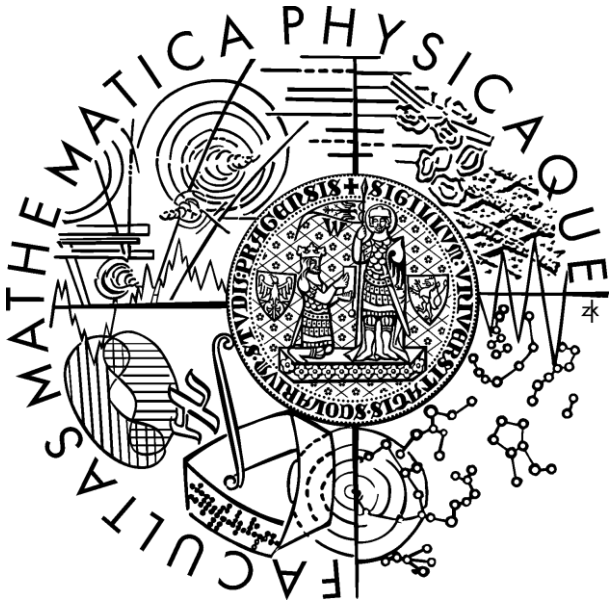

Bc. Ivan Ivani

Modern computational techniques for simulations of molecular spectra

Institute of Physics of Charles University

Supervisor: doc. RNDr. Vladimír Baumruk, DrSc.

Consultant: doc. RNDr. Petr Bouř, CSc.

Field of study: Biophysics and Chemical Physics

2010

I would like to thank my supervisor, doc. RNDr. Vladimír Baumruk, DrSc., for his patience, continuous support and help during all the period of my work on the thesis. I am also grateful to doc. RNDr. Petr Bouř, CSc., who consulted my work and from whom I have learned so much.

Prohlašuji, že jsem svou diplomovou práci napsal samostatně a výhradně s použitím citovaných pramenů. Souhlasím se zapůjčováním práce.

I hereby confirm that the diploma thesis submitted is entirely my own work and all other sources used are cited appropriately. I agree with lending of the thesis.

Prague, 16th April 2010 Bc. Ivan Ivani

Contents

Title: Modern computational techniques for simulations of molecular spectra
Author: Bc. Ivan Ivani
Department: Institute of Physics of Charles University
Supervisor: doc. RNDr. Vladimír Baumruk, DrSc.
Supervisor's e-mail address: vladimir.baumruk@mff.cuni.cz

Abstract: Accurate computations of vibrational energies and vibrational spectra of molecules require an inclusion of the anharmonic forces. In standard computational protocols, a large vibrational Hamiltonian matrix is diagonalized, and spectral intensities are calculated for individual transitions separately. In this work we propose an alternate direct generation of the spectral curves based on a temporal propagation of a trial vibrational wavefunction followed by a Fourier transformation. The lack of the lengthy and computer-memory demanding diagonalization makes the method suitable for larger molecules. It is especially convenient for sparse Hamiltonians that are commonly obtained within the harmonic oscillator basis set, and the algorithm is amendable to parallelization. On a model water dimer basic convergence properties are discussed. The method is then applied to vibrational Raman intensities of the fenchone compound, were it provides spectral shapes comparable with those obtained by the classical approaches.

Keywords: vibrational spectra, anharmonic corrections, Raman, ROA, Fourier transform method

Název práce: Použití moderních výpočetních metod pro simulace molekulárních spekter
Autor: Bc. Ivan Ivani
Katedra (ústav): Fyzikální ústav University Karlovy
Vedoucí diplomové práce: doc. RNDr. Vladimír Baumruk, DrSc.
e-mail vedoucího: vladimir.baumruk@mff.cuni.cz

Abstrakt: Přesné výpočty vibračních energií a vibračních spekter molekul vyžadují započítání anharmonických sil. Ve standardním výpočetním protokolu, jsou velké vibrační matice Hamiltoniánu diagonalizovány a spektrální intenzity počítány pro jednotlivé přechody odděleně. V této práci navrhujeme alternativní přímé generování spektrálních křivek na základě časové propagace náhodné vibrační vlnové funkce následované Fourierovou transformací. Nedostatek zdlouhavé a výpočetně náročné diagonalizace činí metodu vhodnou pro větší molekuly. Je zvláště vhodná pro velké Hamiltoniány, které jsou běžně získány v rámci báze harmonických oscilátorů, a algoritmus umožňuje paralelizaci. Na modelu dimeru vody jsou diskutovány základní vlastnosti konvergence. Metoda je pak použita na vibrační Ramanovy intenzity fenchonu, kde byly získány spektrální profily srovnatelné s výsledky získanými klasickými přístupy.

Klíčová slova: vibrační spektra, anharmonické korekce, Ramanova spektroskopie, ROA, Fourierova transformační metoda

Chapter 1

Introduction

1.1 Computation of Molecular Vibrational Spectra

To understand and interpret the experimental data, and obtain information about molecular structure, simulations of vibrational spectra are always necessary. For biologically relevant systems, such as, peptides, nucleic acids and others, the vibrational spectroscopy provides information on structural and conformational details [1]. Most of the early theoretical approaches were based on parameterized force fields (FF) [2], but nowadays theoretical spectral analysis is based on precise and fast quantum mechanical computations [3].

Typical procedure for obtaining vibrational spectra consists of a diagonalization of a vibrational Hamiltonian, which provides the transition energies, corresponding to peak positions, and wavefunctions with peak intensities. The diagonalization is usually performed by the inverse iteration in memory, or by the Davidson methods [4]. However, for larger molecules diagonalization becomes compute-demanding. In this work, we propose an alternative generation of the spectral curves based on a temporal propagation of a trial vibrational wavefunction followed by Fourier transformation. Fourier method is convenient for problems when the lines are not needed and the Fourier transformation is faster than the complete diagonalization.

For most applications the harmonic approximation [5], is sufficient and widely used for large system, such as peptides and nucleic acids. For better accuracy and more advanced applications the anharmonic potential parts need to be included [6,7]. In that case the harmonic limit is overcame by advanced computational schemes including vibrational configuration interaction (VCI) [8], vibrational self-consistent schemes (VSCF) [9], many-body perturbation theory (PT) [6] etc.

1.2 Organization of the Thesis

The thesis begins with the common theoretical introduction to molecular vibrations. This chapter explains the basic theory of molecular vibrations and vibrational normal mode coordinates, which are essential in this study. Next chapter is reserved for quantum mechanics and harmonic approximation for a treatment of molecular vibrations. The fourth chapter follows harmonic approximation with the expansion to anharmonicity and anharmonic corrections to molecular potential. We briefly explain perturbation theory (PT2), vibrational self-consistent field (VSCF) and vibrational configuration interaction (VCI) theories.

The second part is focused on Raman scattering and Raman optical activity (ROA). Fifth chapter contains an introduction to Raman scattering, Raman spectroscopy, optical selection rules and ROA theory. Also Prague ROA spectrometer is briefly described, as well as results from an experiment of fenchone enantiomers measured at the Institute of Physics at Charles University under supervision of doc. RNDr. Vladimír Baumruk, DrSc.

Finally, last part deals with Fourier transform method and spectra calculated by means of this method. First, the theory of Fourier transform method is explained followed by its implementation into Fortran code and adjustment for various vibrational spectra. Calculations have been done on water dimer to test convergence parameter of the method; also some convergence parameters have been tested on fenchone as well. Last, but most important are the results of the calculations using this method and combining it with anharmonic approximations. The calculations are done for (1S) enantiomer of fenchone and compared with experimental ROA and Raman spectra of fenchone shown in chapter 5.5. The calculations have been done at Institute of Organic Chemistry and Biochemistry under supervision of doc. RNDr. Petr Bouř, CSc.

Last, but not least, are the discussion and conclusion of the method, its advantages for generation of molecular vibrational spectra and possible future tasks.

Chapter 2

Molecular Vibrations

2.1 The Classical Approach to the Vibrational-Rotational Problem of a Polyatomic Molecule

For an interpretation of the infrared and Raman spectra of polyatomic molecules we are primarily interested in the vibrational motions. For convenient computations, we wish to find a way of separating the overall motion into translations, rotations and vibrations.

Let us consider a molecule as a rigid body consisting of N particles with geometry shown on Fig. 2.1. The origin of the moving axes x, y, z is by definition at the center of mass of the molecule. Let us denote by $\mathbf{r}_s$ the position vector of the s-th particle (atomic nucleus or electron) with respect to the x, y, z axis system. Then the following relationship stands for the coordinates of the s-th particle with respect to the transitional and space-fixed axis systems (X, Y, Z):

$$\mathbf{R}_s = \mathbf{R}_0 + \mathbf{S}^{-1}(\vartheta, \phi, \chi) \cdot \mathbf{r}_i \tag{2.1}$$

where $\mathbf{S}(\theta,\varphi,\chi)$ is the three-dimensional orthogonal transformation matrix known from derivation of the Euler angles [see Ref. [5], Appendix A]. $\mathbf{R}_s$ is a column matrix of the components of the position vector of the s-th particle with respect to X, Y, Z, $\mathbf{R}_0$ is the column matrix of the position vector of the origin of the x, y, z axis system with respect to the X, Y, Z axis system (Fig.2.1).

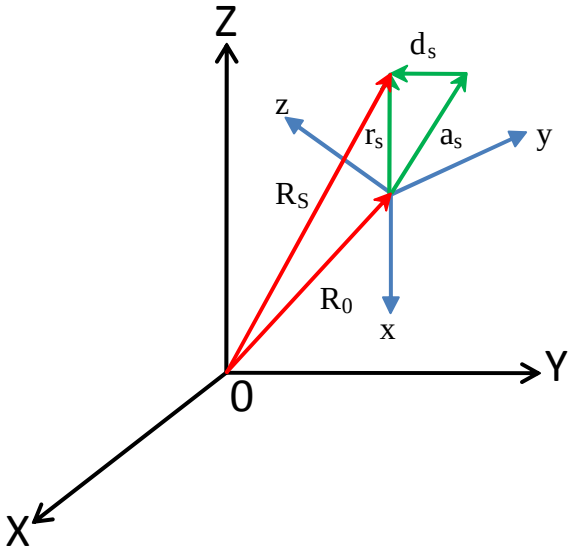

Figure 2.1. *The space-fixed axis system X, Y, Z and the molecule-fixed axis system x, y, z*

A reference configuration of the particles or atomic nuclei of the molecule will now be defined by means of N position vectors $\mathbf{a}_i$ ($i=1,2...N$) which denote the positions of the atomic nuclei with respect to x, y, z axes. It is possible to choose a different reference configuration which corresponds to the minimum of the potential energy of the molecule in a given electronic state. This configuration is called the equilibrium configuration of the atomic nuclei and it can be defined by means of

$$\mathbf{r}_i = \mathbf{a}_i + \mathbf{d}_i \ , \tag{2.2}$$

where $\mathbf{d}_i$ denotes the vector of the Cartesian displacement of the i-th atomic nucleus with respect to the reference configuration (Fig. 2.2).

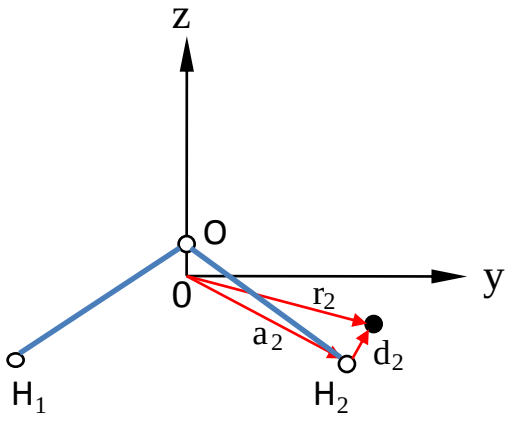

Figure 2.2. *The equilibrium reference configuration (empty dots) and an instantaneous configuration (full dot) of the atomic nuclei of H_2O*

2.2 Eckart Conditions

Considering again the set of 3*N* equations (2.1) for *N* atomic nuclei one can notices that on the left side of the equation are 3*N* variables $R_{i\alpha}$ (i=1,2…N; $\alpha = x, y, z$) while for a nonlinear rigid molecule there are 3*N* + 6 variables on the right side of the equation [3 coordinates of the center of mass, 3 Euler angles and 3*N* Cartesian displacements $d_{i\alpha}$]. In order to equalize these numbers of independent variables on both side it is necessary to introduce six constraints for 3*N* variables $d_{i\alpha}$. To achieve this we will use Eckart conditions

$$\sum_{i=1}^{N} m_i \mathbf{d}_\mathbf{i} = 0 \tag{2.3a}$$

$$\sum_{i=1}^{N} m_i (\mathbf{a}_\mathbf{i} \times \mathbf{d}_\mathbf{i}) = 0 \tag{2.3b}$$

The first condition Eckart condition (2.3a) specifies that during a molecular vibration the center of mass of the molecule must remain unshifted. Eq. (2.3b) is the second Eckart condition and means that the vibrational angular momentum is zero. By use of these constraints we arrive to the expression of the total kinetic energy as

$$2T = \dot{R}_s^{\,2} \sum_\alpha m_\alpha + \sum_\alpha m_\alpha (\boldsymbol{\omega} \times \mathbf{r}_\alpha) \cdot (\boldsymbol{\omega} \times \mathbf{r}_\alpha) + \sum_\alpha m_\alpha \dot{\mathbf{d}}_\alpha^2 + 2\boldsymbol{\omega} \cdot \sum_\alpha m_\alpha \mathbf{d}_\alpha \times \dot{\mathbf{d}}_\alpha \tag{2.4}$$

Therefore, the separation of the kinetic energy into pure translational, rotational and vibrational terms is possible only if the last term in (2.4), called the *Coriolis energy*, is neglected. However, in comparison to the pure vibrational term the Coriolis energy is usually smaller and does need to be considered in the vibrational part.

2.3 Normal coordinates

As a consequence of the Eckart conditions discussed in the previous section, the vibrations of the molecule can be treated separately from the rotational and translational motions, using conditions (2.3a) and (2.3b). To express the equation of motion in more simple and compact form we will use matrix notation in expressing the kinetic energy T and the potential energy V of our molecule.

If we call $\mathbf{q}$ a column vector, with components given by the $3n$ mass-weighted Cartesian displacement coordinates $q_i = \sqrt{m_i d_i}$ then the kinetic energy becomes

$$2T = \tilde{\dot{\mathbf{q}}}\dot{\mathbf{q}} \tag{2.5}$$

For small deviations of the atoms around their equilibrium positions, higher terms in expansion of the potential energy in a power series of the displacement coordinates can be neglected.

$$V = V_0 + \sum_i f_i q_i + \frac{1}{2}\sum_{i,j} f_{ij} q_i q_j + \ higher-order\ terms \tag{2.6}$$

Since we are not interested in absolute energy we chose V_0 to be zero. Further, since the equilibrium configuration is by definition at a minimum, the second term in Eq. (2.6) is also zero. From that and by using Eq. (2.6) can be written as

$$2V = \tilde{\mathbf{q}}\mathbf{F}\dot{\mathbf{q}} \tag{2.7}$$

where $\mathbf{F}$ is a square $3N$ *x* $3N$ symmetric matrix whose elements are the force constants f_{ij}.

If the $\mathbf{F}$-matrix was diagonal, the solution of the vibrational problem would be very simple; we could simply break it into $3N$ separate problems and solve the

Schrödinger's equation for one dimensional harmonic oscillators. Therefore, it is desirable to find a better set of coordinates which can preserve the diagonal form of the kinetic and makes the potential energy matrix also diagonal. Obviously, the Eckart conditions [(2.3a) and (2.3b)] must be satisfied as well.

These new coordinates always exist for the potential in the form (2.7) and they are called *'vibrational normal mode coordinates'*. We define a new column vector **Q** with components given by the 3*n* normal coordinates Q_k which is transformed as

$$\mathbf{Q} = \mathbf{L}^{-1}\mathbf{q} \ , \tag{2.8}$$

where **L** is an orthogonal transformation matrix from the mass-weighted Cartesian to the normal mode coordinates. Furthermore, we can express both Eqs. (2.5) and (2.7) in diagonal form as

$$2T = \widetilde{\dot{\mathbf{Q}}}\mathbf{E}\dot{\mathbf{Q}} \tag{2.9}$$

and

$$2V = \widetilde{\mathbf{Q}}\mathbf{\Lambda}\mathbf{Q} \tag{2.10}$$

where **E** is a unit matrix and **Λ** is a diagonal matrix whose elements are proportional to the squares of the normal mode frequencies

$$\lambda_k = 4\pi^2 \nu_k^2 \, . \tag{2.11}$$

One can easily derive that

$$\tilde{\mathbf{L}}\mathbf{G}^{-1}\mathbf{L} = \mathbf{E} \tag{2.12a}$$

and

$$\tilde{\mathbf{L}}\mathbf{F}\mathbf{L} = \mathbf{\Lambda} \, , \tag{2.12b}$$

where **G** is called the kinematic matrix. Combining (2.12a) and (2.12b) yields

$$\mathbf{L}^{-1}\mathbf{G}\mathbf{F}\mathbf{L} = \mathbf{\Lambda} \, , \tag{2.13}$$

which is an eigenvalue equation. Thus the columns of **L** are eigenvectors and the elements of **Λ** are eigenvalues of the characteristic matrix **GF**.

If matrices **G** and **F** are known for a given molecule, the eigenvalues λ_k from Eq. (2.11) are the solutions of the following secular equation:

$$\left|\mathbf{GF} - \lambda\mathbf{E}\right| = 0\,. \tag{2.14}$$

The **G** matrix elements can be calculated easily from the known geometry and atomic masses of the molecule. For each given solution of Eq. (2.14), i.e. for each normal coordinate Q_k, the molecule undergoes a simple motion in which all nuclei move in phase with the same frequency ν_k but with different amplitudes A_{ik}. This kind of motion is called *normal mode of vibration* or simply a *normal vibration* and the frequency associated with it is called a *normal* or *fundamental frequency of vibration.* The normal mode vibrations can be represented, for example, by arrows at each nucleus showing their relative displacements (Fig. 2.3).

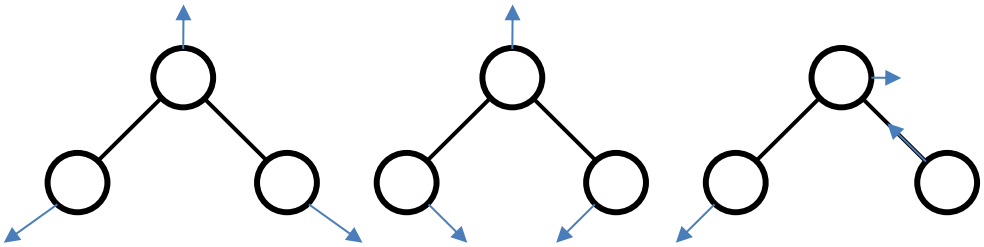

Figure 2.3. *Schematic representation of the normal modes of a non-linear triatomic molecule*

In some cases two or more roots of the eigenvalue equation may coincide and two or more normal vibrations may have the same frequency. These vibrations are called *degenerate* and they are usually related to some symmetry elements in a molecule. When two frequencies are degenerated, then there are only two independent sets of solutions of Eq. (2.13), but an infinite number of ways in which they can be chosen. It is because of the homogeneity of Eq. (2.13).

This method of determining molecular vibrational frequencies is called the **GF** matrix problem or simply *GF method.*

Chapter 3

Quantum Mechanical Approach to Molecular System

3.1 The Born-Oppenheimer Approximation

In the previous chapter we have shown that the classical mechanics approach provides a correct description of the vibration of a polyatomic molecule. In conjunction with the classical electromagnetic theory it can yields general features of the vibrational spectra. It cannot, however, explain many details and fails completely in the explanation of the intensities and fine structure of the vibro-rotational bands. The quantum-mechanical treatment provides not only a correct explanation of such problems, but also provides a consistent picture of electronic, vibrational and rotational spectroscopy.

In quantum mechanics, a polyatomic molecule is described by the complete molecular Hamiltonian *H*. In a stationary state [Eq. (3.1)], a wavefunction ψ and energy value *E* are respectively eigenfunction and eigenvalue of *H*

$$\mathcal{H}\Psi = E\Psi \tag{3.1}$$

where *H* contains terms depending upon the electronic and nuclear coordinates. We want to separate the various contributions to *H,* so that Eq. (3.1) can be divided into two equations and treated separately.

The idea of separating the electronic and nuclear motions comes from the large difference between the mass of the electron and the mass of the nuclei. Since a nucleus is much heavier than an electron, electrons have much larger velocities and move as if the position of the nucleus is fixed. The *Born-Oppenheimer* approximation treats the electronic motions by assuming that the positions of the nuclei is fixed in space which breaks *H* into sum of the electronic (H_e) and nuclear (H_n) Hamiltonian.

$$H = H_e + H_n \tag{3.2a}$$

$$H_n = -\sum_\alpha \frac{\hbar}{2m_\alpha}\frac{\partial}{\partial R_\alpha^2} + \sum_{\alpha,\beta}\frac{Z_\alpha Z_\beta e^2}{R_{\alpha\beta}}$$
$$H_e = -\sum_i \frac{\hbar}{2m_i}\frac{\partial}{\partial r_i^2} + \sum_{i,j}\frac{e^2}{r_{ij}} - \sum_{i,\alpha}\frac{Z_\alpha e^2}{r_{i\alpha}} \qquad (3.2b)$$

where the α and β indexes count nuclei, and *i* and *j* are reserved for electrons. The wavefunction $\psi(\mathbf{r}, \mathbf{R})$, where **r** and **R** are electronic and nuclear coordinates, becomes product of two wavefunctions, the *nuclear* part $\psi_n(\mathbf{R})$, dependent on nuclear coordinates, and the *electronic* one $\psi_e(\mathbf{r}, \mathbf{R})$, parametric dependent on nuclear coordinates.

$$\psi(\mathbf{r},\mathbf{R}) = \psi_e(\mathbf{r},\mathbf{R})\psi_n(\mathbf{R}) \qquad (3.3)$$

The electronic wave equation [Eq. (3.1) for H_e and ψ_e] yields the electronic energy levels, which are important for the electronic spectroscopy. However, we shall limit ourselves to the nuclear Hamiltonian.

From Chapter 2 we know that if we want to separate the nuclear motions into vibrational and rotational motions to a fairly good approximation, we must choose such molecular reference system which satisfies both Eckart conditions, i.e. Eq. (2.3a) and Eq. (2.3b). Such approximation is possible in quantum mechanics as well. If in Eq. (3.2b) we chose a reference system which is located at the center of mass of the molecule, we automatically satisfy the first Eckart condition. Accordingly, if we consider an axis system which rotates with the molecule and satisfies the second Eckart condition, the nuclear Hamiltonian H_n can be written as a sum of H_r, including the interaction of the angular moments of rotation and vibration, and H_v, the vibrational Hamiltonian, which satisfies the equation

$$H_v\psi_v = E_v\psi_v \ . \qquad (3.4)$$

Furthermore, the wavefunction ψ_n can be written as the product of a *rotational* wavefunction ψ_r and a *vibrational* wavefunction ψ_v and more generally as

$$\psi = \psi_e\psi_r\psi_v \ . \qquad (3.5)$$

In some cases, however, the total wavefunction cannot be written as a simple product such as Eq. (3.5) because the Hamiltonian contains interaction terms between different types of coordinates that cannot be neglected. Then the wavefunction is often written as a sum of products of type Eq. (3.5) multiplied by appropriate coefficients [10]

$$\psi = \psi_v \sum_i c_i \psi_{ei} \psi_{ri} \tag{3.6a}$$

$$\psi = \psi_r \sum_i c_i \psi_{ei} \psi_{vi} \tag{3.6b}$$

$$\psi = \psi_e \sum_i c_i \psi_{vi} \psi_{ri} \tag{3.6c}$$

This breaks down the Born-Oppenheimer approximation. For example, the Eq. (3.6a) describes a situation in which rotation-electronic interaction causes the breakdown, etc. Such interactions are of great importance in the analysis of the rotational levels but play relatively minor role in vibrational spectroscopy. Eq. (3.6b) describes a situation in which a vibrational-electronic (vibronic) interaction causes the breakdown, such as in Renner and Jahn-Teller effects (explored in Ref. [2]). Finally, Eq. (3.6c) describes a situation in which a vibro-rotational interaction causes the breakdown, which is the case of the most known Coriolis interaction. The Coriolis interaction can sometimes produce alterations of the absorptions spectra and must be included in calculations of accurate force fields of small molecules.

3.2 The Harmonic Oscillator

As shown in the previous chapters, among a possible set of coordinates for a coordinate system rotating with the molecule and satisfying the Eckart conditions, normal coordinates are by far the most convenient ones since each normal coordinate is associated with one single mode of vibration. Furthermore, the solution of the wave equation expressed in the normal coordinates is rather simple because it can be written as the product of $3N - 6$ one-dimensional harmonic oscillators. Harmonic oscillator in quantum mechanics is a well known problem [11,12].

We briefly recall the one-dimensional harmonic oscillator usage for vibrations. The Hamiltonian is

$$\mathcal{H} = -\frac{\hbar^2}{2}\sum_{i=1}^{3N-6}\left(\frac{\partial^2}{\partial Q_i^2} - \frac{\lambda_i}{\hbar^2}Q_i^2\right) . \tag{3.7}$$

Since the normal coordinates without vibrations/translations represent $3N - 6$ independent variables, the wavefunction ψ of the molecule can be written as a product of $3N - 6$ independent functions $\psi_i(Q_i)$, and the vibrational energy E as a sum of $3N - 6$ terms E_i. We obtain $3N - 6$ independent equations

$$-\frac{\hbar^2}{2}\frac{\partial^2\psi_i}{\partial Q_i^2} + \frac{\lambda_i}{2}Q_i^2\psi_i = E_i\psi_i \quad , \tag{3.8}$$

which are the Schrödinger equations for a one-dimensional harmonic oscillator. Thus we see that the solution of Eq. (3.4) can be expressed as the product of $3N - 6$ harmonic oscillator wavefunctions and the total vibrational energy as the sum of energies of these $3N - 6$ oscillators.

The vibrational energy levels, i.e. the eigenvalues from Eq. (3.8), are

$$E_v^{(k)} = (v_k + \frac{1}{2})h\upsilon_k \tag{3.9}$$

where ω_k is the frequency and v_k is the vibrational quantum number. The solutions are depicted on Figure. 3.1 for $v_i = 0,1,2,3$, together with corresponding wavefunctions $\psi_n(x)$ and spatial probabilities $|\psi_n(x)|^2$.

The wavefunction (see Ref. [5,10,12]) is

$$\psi(Q) = N_v\widetilde{H}_i(\gamma^{1/2}Q)\exp\left(-\gamma\frac{Q^2}{2}\right), \tag{3.10}$$

where $\widetilde{H}_i(Q)$ are the Hermitian polynomials of degree i, $\gamma = 4\pi^2 v_k / h$ and N_v is a normalization constant [5].

This solution of the wave equation expressed in terms of normal coordinates is usable with minor modifications also for degenerate vibrations [10].

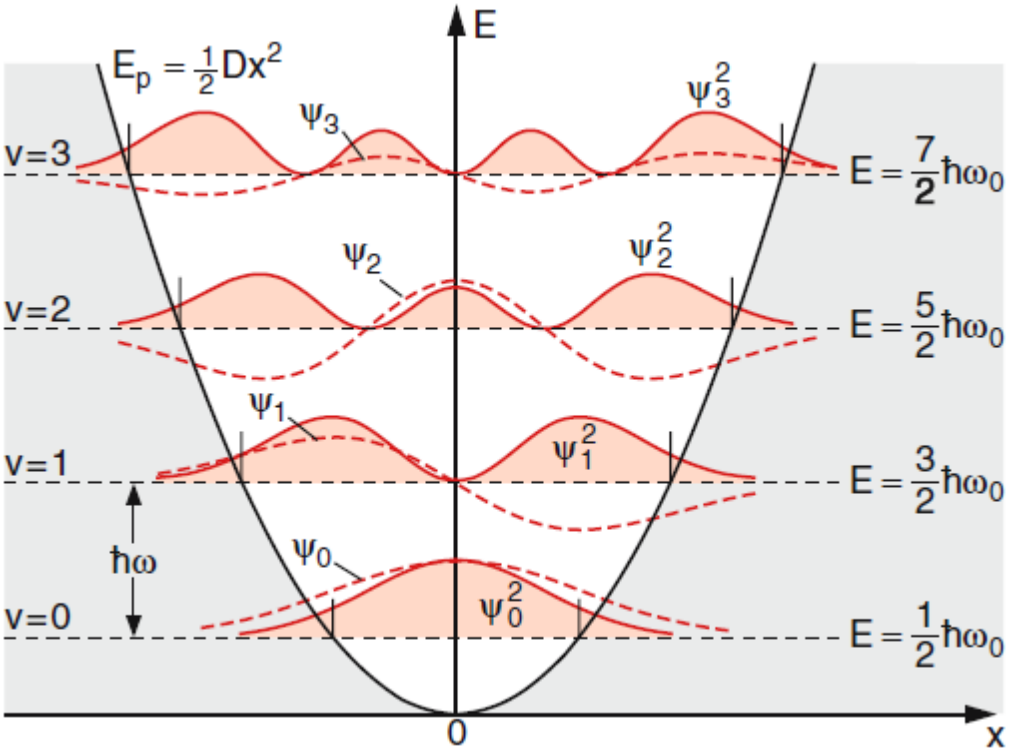

Figure 3.1. *Equidistant energy levels wavefunctions $\psi_n(x)$ and spatial probability $|\psi_n(x)|^2$ for a harmonic oscillator. [13]*

Total vibrational molecular energy is

$$E_v = \sum_{i=0}^{3N-6} (v_i + \frac{1}{2})h\upsilon_i \tag{3.11}$$

From Eq. (3.11) is apparent that for the lowest energy level, all normal modes have zero quantum number. This corresponds to the *zero-point* energy. Important transitions in energy levels are *fundamental transitions, overtone transitions and combination transitions.* In f*undamental transition* all quantum numbers remain zero except one, which becomes equal to unity; while in an *overtone transition* one quantum number changes to higher than unity, i.e. > 1. In *combination transition* two or more quantum numbers are changed.

3.3 The Anharmonic Potential

The potential energy of a molecule is usually written as a Taylor expansion in terms of a set of displacement coordinates (Chapter 2)

$$V = V_0 + \sum_i f_i q_i + \frac{1}{2}\sum_{i,j} f_{ij} q_i q_j + \frac{1}{6}\sum_{i,j,k} f_{ijk} q_i q_j q_k + \frac{1}{24}\sum_{i,j,k,l} f_{ijkl} q_i q_j q_k q_l + \ldots , \qquad (3.12)$$

where the constants

$$f_i = \left(\frac{\partial V}{\partial q_i}\right), \; f_{ij} = \left(\frac{\partial^2 V}{\partial q_i \partial q_j}\right), \; f_{ijk} = \left(\frac{\partial^3 V}{\partial q_i \partial q_j \partial q_k}\right), \; f_{ijkl} = \left(\frac{\partial^4 V}{\partial q_i \partial q_j \partial q_k \partial q_l}\right) \qquad (3.13)$$

are called linear, quadratic, cubic, quartic, etc., force constants and the q_i designate suitable set of displacement coordinates. As discussed before (see Chapter 2), the zero of the energy scale can always be chosen so that V_0 is zero and, furthermore, since the molecule in the equilibrium configuration must be at a minimum of energy, we get

$$\sum_i f_i q_i = 0 . \qquad (3.14)$$

The value of cubic and quartic forces constants is, even for a small molecule, very high, but their contribution to the total energy (3.12) is small for small displacements, in compare to the quadratic term. For these reasons they are generally neglected in the treatment of polyatomic molecules and the potential energy is assumed to be pure quadratic in the displacement coordinates. In this case the potential function is called harmonic (see Chapter 3.2), since it describes harmonic vibrations of the nuclei around equilibrium positions.

If terms higher than the quadratic are retained in (3.12), the potential function is called *anharmonic*, since the equations of motion have in this case different solutions which describe anharmonic motions of the nuclei. This correction can be quite important for vibrations involving the displacement of light atoms, such as hydrogen stretching motions which are of rather large amplitude.

3.4 The Anharmonicity

The harmonic treatment of molecular vibration rests on the assumption of infinitesimal displacements of the nuclei from their equilibrium positions. In this approximation the solution of the vibrational problem is straightforward and can be accomplished with the standard **GF** method outlined in Chapter 2. However, the vibrational spectra of molecular systems show definite deviations from the predictions of the harmonic model. The most important are:

(1) The harmonic model predicts that the vibrational levels associated with a given vibrational mode should have a constant spacing, i.e. that overtones corresponding to quantum jumps $\Delta\upsilon = 2,3,etc.$, should occur at frequencies which are exactly twice, three times, etc., the frequency of the fundamental mode.

(2) The Teller-Redlich product rule is never exactly satisfied by experimental frequencies of isotopic molecules. Differences up to some percent are normally observed.

(3) The selection rules for the harmonic oscillator predict that for small displacements of the nuclei, overtones and combination bands should be forbidden in the vibrational spectrum. However, in measured spectra such bands are often observed.

In order to interpret these experimental results it is necessary to drop the assumption of small displacement of the atoms and to use a more complex model in which terms higher than the quadratic are retained in the potential function expansion (3.12).

The main difficulty associated with the anharmonic model is that it cannot be treated just as an extension of the harmonic one. First of all, when terms higher than the quadratic are retained in the Taylor expansion of the potential, i.e. Eq. (3.12), the Schrödinger equation cannot be solved exactly and approximate methods must be used. In the next section we shall present quantum-mechanical treatment of the anharmonic oscillator.

Chapter 4

Anharmonic Approximations

4.1 Second-Order Perturbation

If the potential function (3.12) is introduced into the Schrödinger equation (3.1) an exact solution of the type obtained for the harmonic oscillator [Eq. (3.11)] cannot be found. However, one can take advantage of the fact that for small displacements of the nuclei the quadratic part of the potential is much larger than the cubic and quartic. On this basis the vibrational Hamiltonian can be divided into orders of magnitude and perturbation theory can be used to calculate the corrections to the vibrational energy due to the certain terms.

If we limit ourselves to molecules with non-degenerate vibrations we write the potential and the energy in orders of magnitude in the form

$$V = V^{(0)} + \lambda V^{(1)} + \lambda^2 V^{(2)} \tag{4.1a}$$

$$E = \sum_i hc\upsilon_i (v_i + \frac{1}{2}) + \lambda E^{(1)} + \lambda^2 E^{(2)} \ , \tag{4.1b}$$

where

$$V^{(0)} = \frac{1}{2} hc \sum_i \upsilon_i q_i^2 \tag{4.2a}$$

$$V^{(1)} = hc \sum_{ijk} f_{ijk} q_i \, q_j q_k \tag{4.2b}$$

$$V^{(2)} = hc \sum_{ijkl} f_{ijkl} q_i \, q_j q_k q_l \tag{4.2c}$$

and λ is a parameter defining the order of magnitude of the various terms. We obtain from Rayleigh-Schrödinger perturbation theory treatment [12] that the corrections to the energy to first and second order are given by

$$\text{First order } E^{(1)} = \sum_m \langle m | V^{(1)} | m \rangle \tag{4.3a}$$

$$\text{Second order } E^{(2)} = \sum_m \left[\langle m | V^{(2)} | m \rangle + \sum_{n \neq m} \frac{\langle m | V^{(1)} | n \rangle \langle n | V^{(1)} | m \rangle}{E_m^0 - E_n^0} \right] \tag{4.3b}$$

In these expressions $\langle m |$ and $\langle n |$ indicate the complete zero-order vibrational wavefunctions corresponding to the vibrational zero-order energies E_m^0 and E_n^0, respectively. According to Chapters 2.3 and 3.2, these functions are the product of $3N - 6$ harmonic oscillator wavefunctions, each depending upon one single normal coordinate Q_i and defined by one single quantum number υ_i. For the simplicity we can express the harmonic oscillator wavefunctions by their quantum number and implement it in Eqs. (4.3a) and (4.3b). One can find this in Ref. [5,10].

Since the matrix elements of the type

$$\langle \upsilon_i | q_i | \upsilon_i \rangle \tag{4.4}$$

are always equal to zero [10], we conclude that the first-order correction to the energy, i.e. Eq. (4.3a), which involves only diagonal matrix elements of the type (4.4), is equal to zero.

The second-order correction to the energy, i.e. the Eq. (4.3b), is made of two parts.The first part involves the diagonal matrix elements of the second-order perturbation terms $V^{(2)}$ and the second, which is involving off-diagonal matrix elements of the first-order perturbation term $V^{(1)}$. The division by the energy difference in Eq. (4.3b) makes the second-order perturbation numerically unstable because of random degeneracies (see Chapter 2.3). Simple treatment based on separation of the degenerate and non-degenerate states was proposed by Matsunaga at al. [14].

For Raman scattering, which will be discussed in next chapter, second-order perturbation correction has to be used because of the nature of the Raman effect. The

interaction of radiation with matter can be discussed in two different ways; *semiclassical*, which considers classical concept of the radiation field and quantum mechanics material system; *quantum field*, which treats both the molecule and the radiation field as quantized system. Both treatments are based on time-dependent perturbation theory. Since the scattering is *two-photon* process, it requires second-order perturbation theory to be fully described.

4.2 Vibrational Self-Consistent Field

The Vibrational Self-Consistent Field calculation (VSCF) [9,14] starts with the vibrational normal modes of the molecule at the molecular equilibrium geometry (see Chapter 2.3). By using Born-Oppenheimer approximation (see Chapter 3.1) we obtain a vibrational Schrödinger equation for non-rotating molecule as

$$\left[-\frac{1}{2}\sum_{i=1}^{N}\frac{\partial^2}{\partial Q_i^2}+V(Q_1,...,Q_N)\right]\Psi_N(Q_1,...,Q_N)=E_N\Psi_N(Q_1,...,Q_N) \qquad (4.5)$$

for number of modes N, where Q_j is the jth normal coordinate. Equation (4.5) neglects vibrational-rotational coupling [15], which in some cases can play an important role, even for $J = 0$ states.

The harmonic approximation (see Chapter 3.2) is not used, however, the VSCF method approximates the total wavefunction by the product of single-mode wavefunctions $\psi_i(Q_i)$ for the mode i:

$$\Psi_N(Q_1,...,Q_N)=\prod_{i=1}^{N}\psi_i(Q_i)\,. \qquad (4.6)$$

and the potential as a sum of effective potentials $v_i(Q_i)$,

$$V(Q_1,...,Q_N)\rightarrow\sum_{i=1}^{N}v_i(Q_i) \quad , \qquad (4.7)$$

which are given by

$$v_i(Q_i)=\left\langle\prod_{l\neq i}^{N}\psi_l(Q_l)\middle|V(Q_1,...,Q_N)\middle|\prod_{l\neq i}^{N}\psi_l(Q_l)\right\rangle. \qquad (4.8)$$

The effective potential $v_i(Q_i)$ can be interpreted as the potential energy of the *i*th mode interacting with the average field of all other modes.

By substituting Eq. (4.6) and (4.8) into Eq. (4.5) and integrating over ψ_l, where $l \neq i$, one can arrive at a set of single-mode VSCF equations,

$$\left[-\frac{1}{2}\sum_{i=1}^{N}\frac{\partial^2}{\partial Q_i^2} + v_i(Q_i) \right]\psi_i(Q_i) = \varepsilon_i \psi_i(Q_i) \ , \tag{4.9}$$

where *i = 1,...,N*. The integral (4.8) depends on $\psi_l(Q_l)$; therefore, the solving of the single-mode vibrational Schrödinger equation must be repeated *"self-consistently"* until the energy values (ε_i) stabilize. The total energy of the system is expressed as a trace of single-mode energy ε_i:

$$E_N^{VSCF} = \sum_{i=1}^{N}\varepsilon_i - (N-1)\left\langle \prod_{i=1}^{N}\psi_i(Q_i) \middle| V(Q_1,...,Q_N) \middle| \prod_{i=1}^{N}\psi_i(Q_i) \right\rangle . \tag{4.10}$$

The second term in Eq. (4.10) represents self-interaction correction term due to double counting of the off-diagonal interaction potentials in the Hamiltonian.

As the excited states can be treated only approximately within the VSCF scheme two alternative approaches were proposed by Daněček and Bouř [6]. In the first approximation, only the ground states wavefunctions $\psi_i(Q_i)$ were used for determining the potential from Eq. (4.7) (referred to as **gVSCF**), while in the second approximation (referred as **eVSCF**) excited states were included in the averaging. The **gVSCF** computation requires only one set of the self-consistent iterations for the ground state, while this has to be repeated for each excited state in **eVSCF**.

The effect of correlation between different modes as a correction to VSCF can be obtained by means of the second-order perturbation theory, known as Møller-Plesset pertubationing [16] or MP2, that has been known to be reliable and computationally less demanding than methods such as the configuration interaction (CI). It has been shown that *Correlation-corrected* VSCF (**CC-VSCF**) improves the accuracy [17]. The perturbation correction to the VSCF is also reliable and can be computed with efficiency. The procedure is similar to one showed in previous

paragraph, except that for the VSCF wavefunction, the perturbation is defined as a difference between the exact (Eq. 3.12) and the VSCF potential (Eq. 4.9),

$$W = V - \sum_{i=1}^{N} v_i \tag{4.11}$$

A second-order correction can be obtained from a standard perturbation calculus as

$$E_n^{(2)} = \sum_{m \neq n} \frac{|W_{nm}|^2}{E_n - E_m} \ , \tag{4.12}$$

where $W_{nm} = \langle n|W|m\rangle$. Just as mentioned in previous paragraph, the division by the energy difference in Eq. (4.12) makes the **PT2** numerically unstable because of random degeneracies.

In a paper by Daněček and Bouř [6] a new modified algorithm was introduced to separate degenerate and non-degenerate states, in which instead of term (4.12) they introduced a different term for all states as

$$E_n^{(2)} = \frac{1}{2} \sum_{m \neq n} \left[E_m - E_n + W_{mm} - W_{nn} \pm \sqrt{\left(E_m - E_n + W_{mm} - W_{nn}\right)^2 + 4|W_{nm}|^2} \right] \tag{4.13}$$

where the + sign holds for $E_n > E_m$ and – sign for $E_n < E_m$. In this way the exact solutions for two-state (*n*,*m*) system includes the degenerate case, while for small perturbations, where $W \rightarrow 0$, its polynomial expansion is equal to Eq. (4.5) up to the second power of *W*.

4.3 Vibrational Configuration Interaction

The VCI method, where the wave function is expressed as a sum of the harmonic oscillator functions, is probably the most universal and most straightforward procedure. Unlike for the VSCF and PT approaches, fundamental and combination energy spectral transitions can be obtained at the same time. Although it may become impractical for large systems [6], it represents an important benchmark as it is, in principle, equivalent to the exact Schrödinger solution.

By assuming the wavefunction as a sum of harmonic oscillator functions, a solution of the Schrödinger equation is directly obtainable from the Hamiltonian diagonalization. This method is clearly limited by the size of the Hamiltonian matrix that has to be diagonalized. For that reason, number of the harmonic states (*i*) that do not play a significant role must be restricted. This selection of the states can be done by introducing a ratio

$$\eta = \left| \frac{W_{fi}}{E_f - E_i} \right| \tag{4.14}$$

so that only values bigger than given limit for at least some ground state or excited state f are concerned for the diagonalization. In addition, the speed of the diagonalization, scaled as N^3, becomes a limiting factor in case of large molecules. Thus some selection of the states is always necessary.

Chapter 5

The Raman scattering

5.1 The interaction between the radiation field and a molecule

Raman spectroscopy has proved to be a powerful tool for investigating the vibrational structure of molecules in their electronic ground state. We shall see that this method is often complementary to infrared spectroscopy. Raman spectroscopy is based on the inelastic scattering of light by molecules and was first discovered by *Chandrasekhara Raman* in 1928.

In the context of photons Raman scattering can be described as a collision of photon $\hbar\omega_0$ with a molecule on the initial level E_i, where part of photon's energy is transferred to the internal energy of the molecule, which is excited to the final level E_f, while the scattered photon $\hbar\omega_s$ has lower frequency (Figure 5.1a). The energy difference $\Delta E = E_i - E_f$ may appear as vibrational, rotational or electric energy of the molecule. The inelastic scattered radiation is called *Stokes radiation*.

If the photon $\hbar\omega_0$ is scattered by an excited molecule and the excitation energy is transferred to the scattered photon, which now has a higher energy that the incident photon (Figure 5.1b). This super-elastically scattered radiation is called *anti-Stokes radiation*. If the incident photon $\hbar\omega_0$ is scattered with the same energy, i.e. the same frequency, then the radiation is elastic and the scattering is called *Rayleigh scattering*.

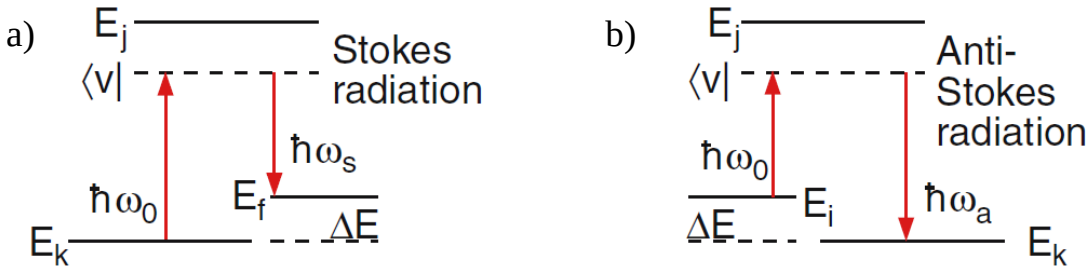

Figure 5.1. *Level scheme for the generation of (**a**) Stokes radiation and of (**b**) anti-Stokes radiation. [13]*

Thus, the spectrum of scattered light consists of these three types of scattering (Figure 5.2).

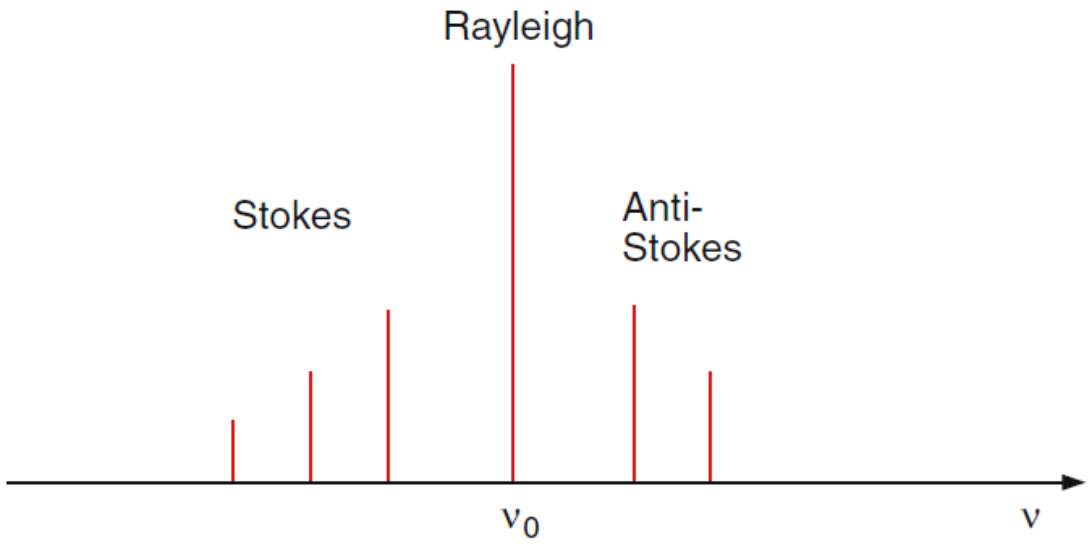

Figure 5.2. *Schematic spectrum of elastic Rayleigh scattering and Raman scattering with Stokes and anti-Stokes lines. [13]*

The classical description of the Raman effect starts with the electric dipole moment

$$\boldsymbol{\mu}(\mathbf{E}) = \boldsymbol{\mu}_0 + \vec{\alpha}\mathbf{E} \tag{5.1}$$

written as the sum of an eventual permanent moment $\boldsymbol{\mu}_0$ and a field-dependent contribution $\boldsymbol{\mu}_{\text{ind}} = \vec{\alpha}\mathbf{E}$, where $\vec{\alpha}$ is the electric polarizability. The dipole moment and the polarizability can both depend on the nuclear displacements q_n of the vibrating molecule. Just as we did for potential (3.12), we can expand dipole moment and polarizability into the Taylor series around equilibrium position as

$$\mu_i(q) = \mu_i(0) + \sum_{n=1}^{3N-6} \left(\frac{\partial \mu_i}{\partial q_n} \right)_0 q_n + \ldots \tag{5.2}$$

$$\alpha_{ij}(q) = \alpha_{ij}(0) + \sum_{n=1}^{3N-6} \left(\frac{\partial \alpha_{ij}}{\partial q_n} \right)_0 q_n + \ldots \quad , \tag{5.3}$$

where $3N - 6$ is the number of normal vibrational modes and $\mu(0)$, and $\alpha_{ij}(0)$, represent dipole moment, and polarizability at the equilibrium position $q = 0$, respectively.

If we describe the nth normal vibration and electric field amplitude as harmonic oscillations around equilibrium position as

$$q_n(t) = q_{n0} \cos(\omega_n t) \tag{5.4}$$

$$\mathbf{E(t)} = \mathbf{E_0} \cos \omega t \tag{5.5}$$

and insert them into (5.1) we obtain

$$\begin{aligned} \mu_i(t) = \mu_i(0) + \sum_{n=1}^{3N-6} \left(\frac{\partial \mu_i}{\partial q_n} \right)_0 q_{n0} \cos(\omega_n t) + \alpha_{ij} E_{0_i} \cos \omega t \\ + \frac{1}{2} E_{0_i} \sum_{n=1}^{3N-6} \left(\frac{\partial \alpha_{ij}}{\partial q_n} \right)_0 q_{n0} \left(\cos(\omega + \omega_n)t + \cos(\omega - \omega_n)t \right) \end{aligned} \quad . \tag{5.6}$$

The first term represent the permanent dipole moment of the molecule. The second term is responsible for the infrared spectrum, where the intensities of the transitions depend on the derivatives $\partial \mu_i / \partial q_n$ [5, 13]. The third term is responsible for the elastic Rayleigh scattering, while the last term describes the Raman scattering, where the intensities of the Raman lines depend on the derivatives $\partial \alpha_{ij} / \partial q_n$.

Figure 5.3 demonstrates the dependences $\partial \mu_i / \partial q_n$ and $\partial \alpha_{ij} / \partial q_n$ on spectral activity for the three normal vibrations of the linear CO_2 molecule.

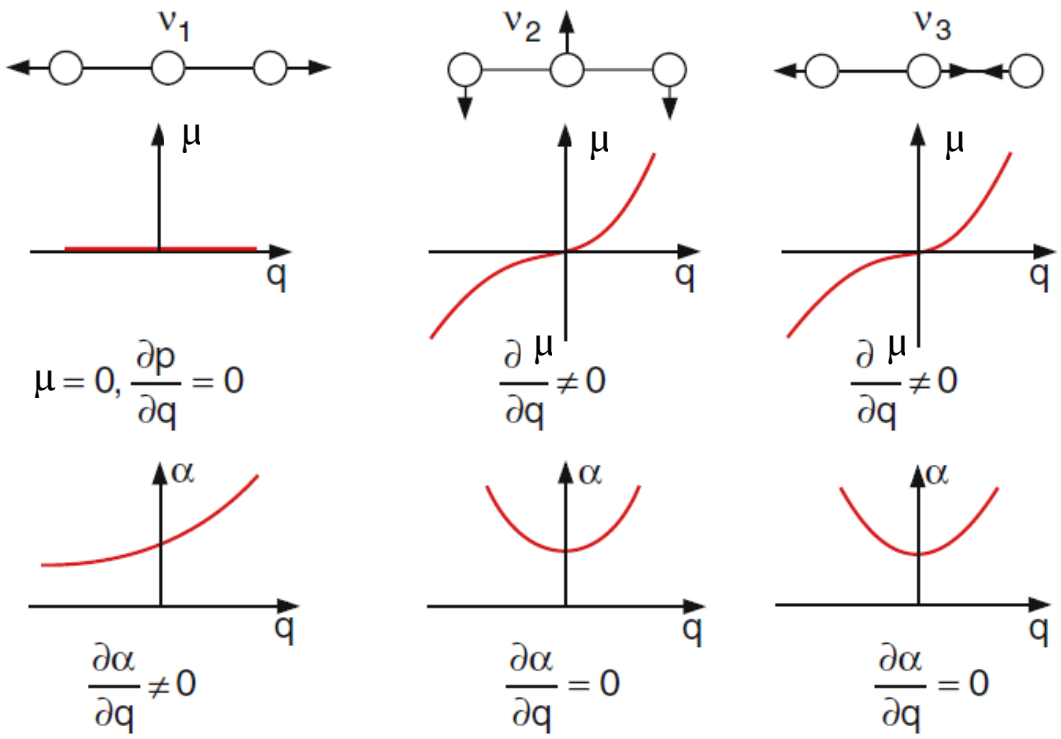

Figure 5.3. *Dependence $\partial\mu_i / \partial q_n$ of dipole moment and $\partial\alpha_{ij} / \partial q_n$ of polarizability on the normal mode vibrations of the molecule CO_2.*

The change of the dipole moment with the vibrational displacements is only nonzero for the bending vibrations υ_2 and for the asymmetric stretching vibration υ_3. These normal modes are therefore called *infrared active*. On the other hand the polarizability changes for the symmetric stretching vibration υ_1, which is called *Raman active*. This demonstrates the infrared and Raman spectroscopy are complementary to each other.

There are many molecules with vibrational modes that are infrared as well as Raman active. This arises from symmetry selection rules related to molecular symmetry.

5.2 Symmetry Selection Rules

Molecules can be classified according to symmetry elements or operations that leave at least one common point unchanged. This classification gives rise to the point group representation for the molecule. Very useful information about the point group is contained in character tables.

For a fundamental transition to occur by absorption of infrared radiation the transition moment integral must be nonzero. The transition moment integral is of the form:

$$\int \psi_v^0 \mu_k \psi_v^f \, d\tau \; ; \qquad \mu_k = (x, y, z) \; , \tag{5.7}$$

where ψ_v^0 is the wave function for the initial state involved in the transition (usually the ground state), and ψ_v^f is the wave function for the final state involved in the transition (the excited state); μ_k is dipole moment, components (*x, y, z*). If any of these three integrals is nonzero, then the transition moment integral is nonzero and the transition is allowed. We can use symmetry considerations to determine whether the transition moment integral is zero or nonzero, and hence whether the transitions is allowed or forbidden. For the integral to be nonzero, the integrand must be symmetric, i.e. the product within integral (5.7) must be symmetric. The ground state wave function, ψ_v^0, belongs to the totally symmetric representation of the point group. The symmetry representation for the excited state wave function, ψ_v^f, depends on the symmetry of the normal mode vibration to be excited. This leads to a very simple rule for the activity of fundamentals in infrared absorption:

A fundamental transition will be infrared active (that is, give rise to an absorption band) if the normal mode involved belongs to the same irreducible representation as any one or several of the Cartesian coordinates.

For a fundamental transition to occur by Raman scattering of radiation the transition moment integral must be nonzero.

$$\int \psi_v^0 \alpha_{ij} \psi_v^f \, d\tau \; ; \qquad \alpha_{ij} = (x^2, y^2, z^2, xy, xz, yz) \tag{5.8}$$

The symmetry representations for the polarizability is the same as that of quadratic terms involving the Cartesian coordinates, x^2, y^2, z^2, *xy*, *yz*, and *xz*. The requirement that integrals (5.8) be nonzero means that there must be a change in polarizability of the molecule when the transition occurs. This leads to a very simple rule for the Raman activity of fundamentals:

A fundamental transition will be Raman active (that is, give rise to a Raman band) if the normal mode involved belongs to the same irreducible representation as quadratic term of the Cartesian components of the polarizability tensor of the molecule.

Figure 5.4. demonstrates the symmetric stretch in carbon dioxide, which is Raman active because the polarizability of the molecule changes. You can see when you compare the ellipsoid at the equilibrium bond length to the ellipsoid for the extended and compressed symmetric motion

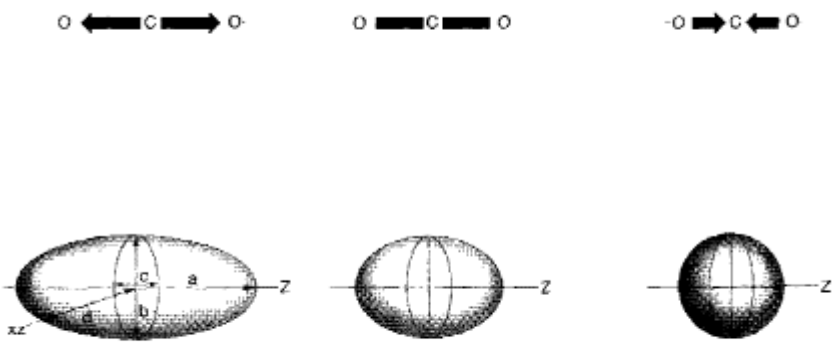

Figure 5.4. *Demonstration change in polarizability ellipsoid of symmetric stretch of carbon dioxide CO_2.*

5.3 Raman Optical Activity (ROA)

Raman optical activity (ROA) is an extension to the Raman scattering that is reliant on the difference in intensity of Raman scattered *right-* and *left-circularly polarized light* due to molecular chirality. The result of ROA measurement gives two spectra – difference spectrum (ROA) and sum spectrum (Raman). ROA is a very weak effect as value Δ from Eq. (5.9) is of the order $\sim 10^{-3}$. The theory was experimentally proven by Barron in 1973 [26] but the expansion of this field came during 1990's mainly because of the usage of multi-channel CCD detectors.

In theory, we introduce a quantity Δ called *circular intensity difference*, which is defined as a ratio of ROA and Raman signal

$$\Delta = \frac{I^R - I^L}{I^R + I^L} \quad , \tag{5.9}$$

where I^R and I^L, are the scattered intensities in right- and left-circularly polarized incident light, respectively. For full description of Raman scattering, an electric dipole approximation was sufficient enough, but to describe ROA effect we go beyond this approximation and include also magnetic dipole and electrical quadrupole terms. These contributions can be expressed with a tensor of molecular polarizability $\alpha_{\alpha\beta}$ (electric dipole – electric dipole) and two tensors of optical activity $G'_{\alpha\beta}$ (electric dipole – magnetic dipole) and $A_{\alpha\beta\gamma}$ (electric dipole – electric quadrupole). In that sense the Eq. (5.9) for isotropic ensemble of chiral molecules measured in ICP (incident circular polarization) ROA in backscattering geometry (see Chapter 5.4) transformers into

$$\Delta = \frac{I^R - I^L}{I^R + I^L} = \frac{48\left[\beta\left(G'\right)^2 + \frac{1}{3}\beta\left(A\right)^2\right]}{2c\left[45\alpha^2 + 7\beta\left(\alpha\right)^2\right]}, \tag{5.10}$$

where α is isotropic invariant of the tensor of polarizability , $\alpha = (1/3)\alpha_{\alpha\alpha} = (1/3)\left(\alpha_{xx} + \alpha_{yy} + \alpha_{zz}\right)$ and $\beta\left(\alpha\right)^2$, $\beta\left(G'\right)^2$ and $\beta\left(A\right)^2$ are anisotropic invariants of the tensor of polarizability and tensors of optical activity, $\beta\left(G'\right)^2 = (1/2)\left(3\alpha_{\alpha\beta}\alpha_{\alpha\beta} - \alpha_{\alpha\alpha}\alpha_{\beta\beta}\right)$ and $\beta\left(A\right)^2 = (1/2)\omega\alpha_{\alpha\beta}\varepsilon_{\alpha\gamma\delta}A_{\gamma\delta\beta}$ [27]. This equation is valid for Rayleigh scattering, but to convert it for Raman scattering one must substitute tensors of molecular properties with Raman tensors of vibrational transition between ground and excited vibrational states n_v and m_v. For example, $\alpha_{\alpha\beta}$ is substituted with $\langle n_\upsilon \left|\alpha_{\alpha\beta}\right| m_\upsilon \rangle$.

5.4 Experimental arrangement in ROA spectroscopy

Typical ROA spectrometer consists of incident laser (mostly argon laser), fast imaging spectrograph and cooled CCD detector. In ICP ROA spectrometer (see Fig. 5.5) incident light is modulated by electro-optical modulator (Pockels cells), which switches between right- and left-circularly polarized incident light. In contrast, SCP (scattered circular polarization) ROA is based on polarization splitter, which separates right and left circularly polarized components of the scattered light.

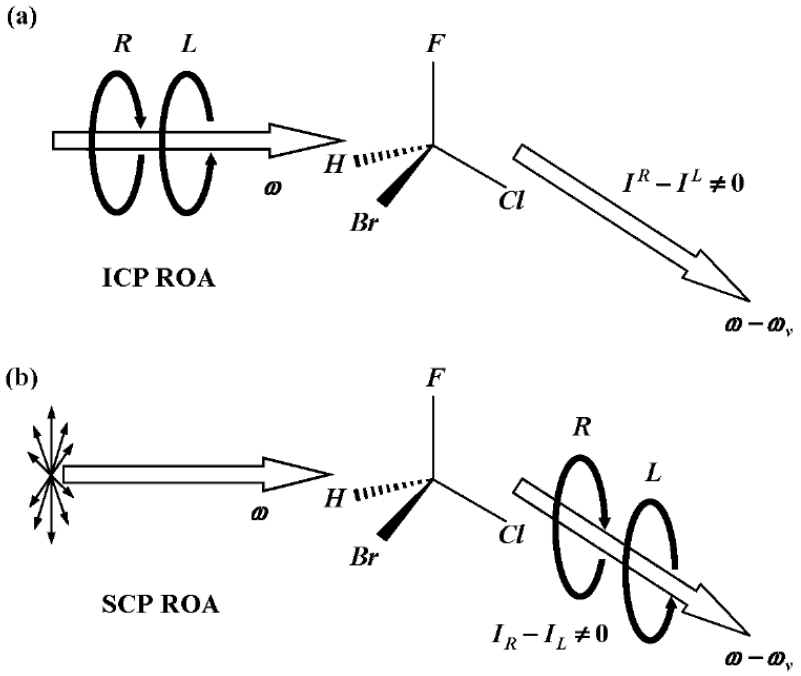

Figure 5.5. *Two equivalent ROA experiments: (a) in ICP ROA arrangement* $I^R - I^L$ *is measured, where* I^R *and* I^L *are intensities of scattered non-polarized light from right- and left-circularly polarized incident light, respectively. (b) in SCP ROA arrangement* $I_R - I_L$ *is measured, where* I_R *and* I_L *are intensities of right- and left-circularly polarized components of scattered light, respectively, while incident light is linear or unpolarized.*

Prague ROA spectrometer at the Institute of Physics of the Charles University (Fig. 5.6) was inspired by apparatus from L. D. Barron's group at University of Glasgow. Apparatus uses variant ICP in backscattering geometry with electro-optical modulator (EOM), which allows switching between right- and left-circularly polarized light. More details about the apparatus can be found in doctoral thesis of J. Kapitán [28].

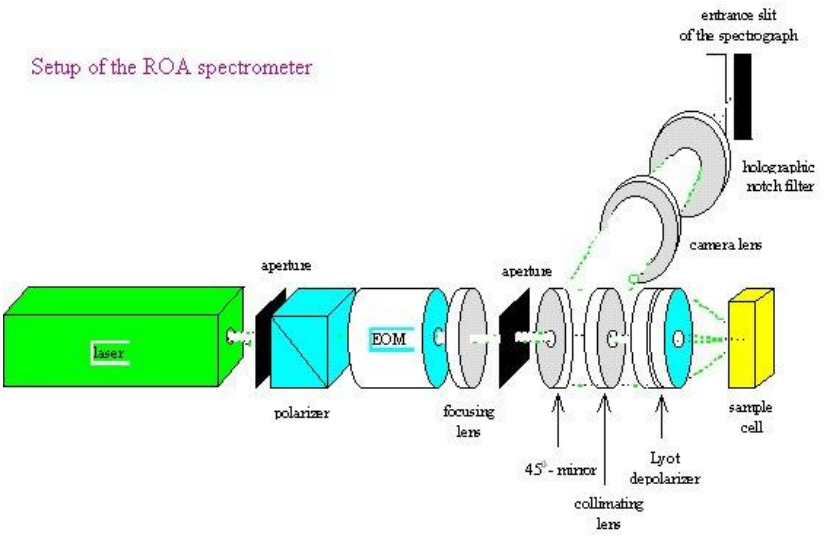

Figure 5.6. *Arrangement of ICP ROA spectrometer for backscattering geometry built at the Institute of Physics of the Charles University in Prague.*

5.5 Results

At first I was introduced in detail to spectrometer shown on Fig. 5.6. After that I did a test measuring on α-pinene with exposure of 0.5s, 250 accumulations and 2 frames. Then I prepared 1ml of (1S)-(+) and (1R)-(-) fenchone enantiomers into centimeter's cuvette. Fenchone enantiomers were measured with 0.4s exposure, 300 accumulations and 4 frames. Their Raman and ROA spectra are pictured on Fig. 5.8. Clearly, Raman spectrum of (1S)-(+) enantiomer have a fluorescent background and cannot be used for theoretical comparison. For that reason, we used data that were measure by M. Kubáňová that were published in her diploma thesis from 2009 [29].

Fenchone is natural organic compound classified as a monoterpene and a katone. It is a colorless oily liquid. Fenchone is a constituent of absinth and the essential oil of fennel and it is used as a flavor in foods and in perfumery. It has two enantiomers (1S) and (1R) which are shown in Fig. 5.7.

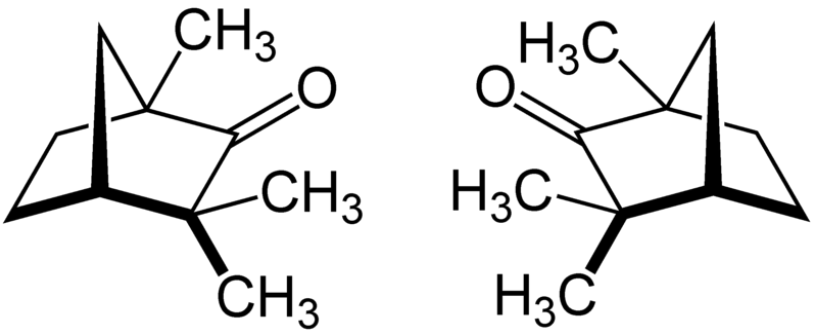

Figure 5.7. *Fenchone enantiomers' structural formulas. (1S)-(+) (left) and (1R)-(-) (right) [18].*

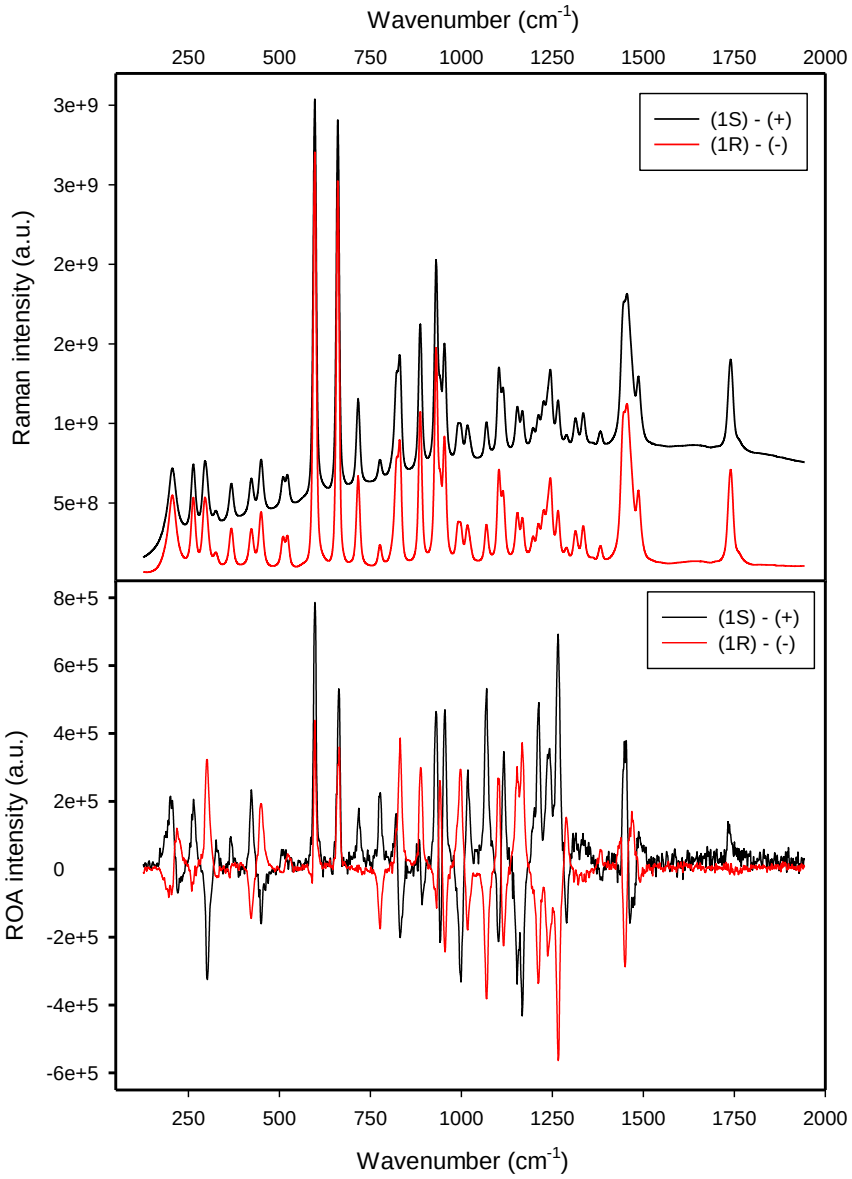

Figure 5.8. *Raw Raman and ROA spectra of fenchone enantiomers (1S) and (1R) measured in ICP ROA backscattering geometry with 0.4s exposure, 300 accumulations and 4 frames.*

Chapter 6

Fourier Transform Method

6.1 Introduction

In standard computational protocols of the vibrational spectra, a large vibrational Hamiltonian matrix is diagonalized, and spectral lines are calculated for individual transitions separately. For large Hamiltonian matrixes this becomes a problem as the lengthy diagonalization of the large matrixes makes the computation more demanding. We propose an alternate direct generation of the spectral curves based on a temporal propagation of a trial vibrational wavefunction followed by a Fourier transformation. The lack of the computer-memory demanding diagonalization makes the method suitable for large molecules. Fig. 6.1 demonstrates classical approach to molecular vibrational spectra calculation compared with our Fourier transform method.

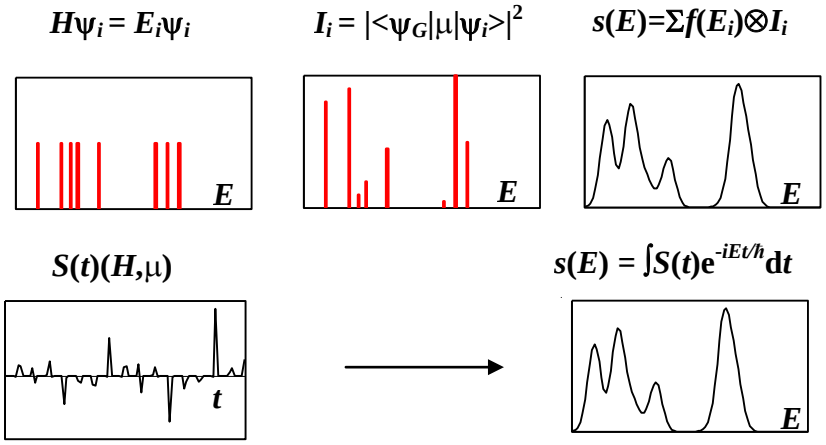

Figure 6.1. *Schematic representation of the two ways of simulating vibrational spectra: (top) by the usual way discrete energies are found by a Hamiltonian (H) diagonalization, the intensities (I) are obtained from the eigenfunctions ψ and dipole moment μ, and the spectrum s(E) is created by a convolution with an arbitrary peak shape f. (Bottom) within the Fourier method, a spectral function (S) is let to develop in time, providing the spectrum in the energy domain.[19]*

6.2 Theory

Let us have a Hamiltonian H and the stationary Schrödinger equation $H|K\rangle = E_K|K\rangle$. Every time-dependent wavefunction can be written as a sum

$$|\psi(t)\rangle = \sum_{K=1,N} d_K |K\rangle e^{-i(E_K t)/\hbar}, \tag{6.1}$$

and propagated according to Schrödinger's time equation $i\hbar\dot{\psi}(t) = H\psi(t)$, so that

$$\psi(t+dt) = \psi(t) + \dot{\psi}(t)dt + \frac{1}{2}\ddot{\psi}(t)dt^2. \tag{6.2}$$

At each step we used $\dot{\psi}(t) = \frac{H}{i\hbar}\psi(t)$, $\ddot{\psi}(t)dt^2 = \psi(t) + \psi(t-2dt) - 2\psi(t-dt)$, and the wavefunction was renormalized.

Further, we suppose that it is relatively easy to obtain vibrational ground state. The harmonic oscillator wavefunction obtained from the harmonic part of the Hamiltonian is usually very close to the true vibrational ground state [5,6]. But also the exact ground state can be obtained by the Davidson diagonalization schemes [4] as the first eigenvector even from large anharmonic Hamiltonians. The ground state wavefunction can be propagated analytically as

$$|\psi_G(t)\rangle = |G\rangle e^{-i(E_G t)/\hbar}, \tag{6.3}$$

where E_G is the ground state energy. Additionally, we propagate a random function $\psi_R = \sum_K d_K^R \psi_K$, and integral

$$\boldsymbol{\mu}_R(t) = \langle \psi_R^*(t) | \hat{\boldsymbol{\mu}} | \psi_G(t) \rangle, \tag{6.4}$$

where $\hat{\boldsymbol{\mu}}$ is the dipole moment operator. Furthermore, we get

$$\boldsymbol{\mu}_R(t) = \sum_K d_K^{R^*} \langle K | \hat{\boldsymbol{\mu}} | G \rangle e^{i\omega_{KG}t}. \tag{6.5}$$

which can be Fourier-transformed as

$$\boldsymbol{\mu}_R(\omega) = \int \boldsymbol{\mu}_R(t) e^{-i\omega t} dt \tag{6.6}$$

$$= 2\pi \sum_K d_K^{R^*} \langle K | \hat{\boldsymbol{\mu}} | G \rangle \delta(\omega_{KG} - \omega) .$$

Than we define an absorption spectrum as

$$I_R(\omega) = \frac{\sqrt{2\pi} dN\omega}{4\pi^2} |\boldsymbol{\mu}_R(\omega)|^2 = \sum_K \langle K|\hat{\boldsymbol{\mu}}|G\rangle . \langle G|\hat{\boldsymbol{\mu}}|K\rangle \omega\delta(\omega_{KG} - \omega) . \tag{6.7}$$

In the derivation of Eq. (6.7) we used an approximate relation

$$\delta(\omega_{KG'} - \omega)\delta(\omega_{K'G'} - \omega) \approx \frac{1}{d\sqrt{2\pi}} \delta_{KK'}\delta(\omega_{K'G'} - \omega) \tag{6.8}$$

valid for approximate "δ-functions" in a form of Gaussian bands with a bandwidth *d*,

$$\delta_d(\omega) \approx e^{-(\omega/d)^2} / (d\sqrt{\pi}) , \tag{6.9}$$

and replaced the state weights by the average, $|d_K^R|^2 = 1/N$. The averaging can be realized by propagating *M* vectors (ideally $M \to \infty$) and averaging the intensities, so that we get the absorption index as

$$\varepsilon(\omega) = \frac{1}{9.184 \times 10^{-3} M} \sum_{R=1,M} I_R(\omega) . \tag{6.10}$$

6.3 Implementation [Ref. 19]

The algorithm derived above was implemented into Petr Bouř's program S4 [20] as follows:

1) Calculate Cartesian derivatives of a dipole (by Gaussian) $\boldsymbol{\mu}_C = \partial\boldsymbol{\mu}/\partial\mathbf{R}$; if required, calculate also second dipole derivatives $\boldsymbol{\mu}_{CC} = \partial^2\boldsymbol{\mu}/(\partial\mathbf{R}\partial\mathbf{R})$, by a numerical differentiation.
2) Transform the first (second) derivatives into the normal mode coordinates (Q),

using the Cartesian-normal mode transformation matrix S, $\boldsymbol{\mu}_Q = \mathbf{S}.\boldsymbol{\mu}_C$ ($\boldsymbol{\mu}_{QQ} = \mathbf{S}.\mathbf{S}\boldsymbol{\mu}_{CC}$).

3) Construct the vibrational Hamiltonian matrix H in the harmonic oscillator basis $\{\varphi_i\}$. In the current work, the Hamiltonian operator was in sense of Eq. (3.12)

$$H = \frac{1}{2}\sum_{i=1}^{M}(P_i^2 + \omega_i^2 Q_i^2) + \frac{1}{6}\sum_{i=1}^{M}\sum_{j=1}^{M}\sum_{k=1}^{M} c_{ijk} Q_i Q_j Q_k + \frac{1}{24}\sum_{i=1}^{M}\sum_{j=1}^{M}\sum_{k=1}^{M}\sum_{l=1}^{M} d_{ijkl} Q_i Q_j Q_k Q_l \tag{6.7}$$

where $P_i = -i\hbar\partial/Q_i$, ω_i are the fundamental frequencies. All cubic (c_{ijk}) and semidiagonal (d_{ijkl}, where at least two indices were the same) constants were included. The size of the Hamiltonian was controlled by skipping of the lowest-frequency modes and by considering harmonic states that significantly interact with the ground or fundamental (F) vibrations ($\left|\langle\varphi_i | V | F\rangle / (E_i - E_F)\right| \geq threshold$, where V are the last two sums in (6.7)). Only non-zero elements of H are stored in a memory.

4) Calculate the ground eigenvector d_G ($|G\rangle = \sum_i d_{G,i}|\varphi_i\rangle$) from $\mathbf{H}.\mathbf{d}_G = E_G\mathbf{d}_G$, by a Davidson iteration.

5) From d_G, calculate vector u_G, $\mathbf{u}_{G,i}(0) = \sum_j d_{G,i}\langle\varphi_j | \hat{\boldsymbol{\mu}} | \varphi_i\rangle$, where $\hat{\boldsymbol{\mu}} = \boldsymbol{\mu}_Q.\mathbf{Q} + (1/2)\mathbf{Q}.\boldsymbol{\mu}_{QQ}.\mathbf{Q}$.

6) Initialize complex spectrum $\boldsymbol{\mu}(\omega) = 0$, set time t = 0 and iteration step k = 0. In a set of complex trial vectors d_R (R = 1...M), set each component $d_{R,i}$ (i=1...N) to a random number within (-0.5...0.5) and normalize, so that $|\mathrm{d}_R|$ = 1.

7) Increment time t by dt and obtain

new vector $\mathbf{d}_R^{(k+1)} = \mathbf{d}_R^{(k)} - (i/\hbar)\mathbf{H}.\mathbf{d}_R^{(k)} + (1/2)\mathbf{d2}_R^{(k)}$,

updated second derivatives $\mathbf{d2}_R^{(k+1)} = (\mathbf{d}_R^{(k)} + \mathbf{d}_R^{(k-2)} - 2\mathbf{d}_R^{(k-1)})/dt$,

and the dipole $\boldsymbol{\mu}_R(t) = \mathbf{d}_R.\mathbf{u}_G e^{-i\omega t}$.

8) Accumulate dipole spectrum $\boldsymbol{\mu}(\omega) = \boldsymbol{\mu}(\omega) + e^{-i\omega t}\boldsymbol{\mu}_R(t)dt$.

9) If $k < ki_{max}$, goto 7.

10) From $\boldsymbol{\mu}(\omega)$, calculate the intensity spectrum according to (6.7) and (6.10).

6.4 Modification of the algorithm for other spectra [Ref. 19]

Raman spectra can be obtained by replacing the dipole operator $\hat{\boldsymbol{\mu}} = \boldsymbol{\mu}_Q \mathbf{.Q} + (1/2)\mathbf{Q}.\boldsymbol{\mu}_{QQ}\mathbf{.Q}$ by molecular polarizability $\hat{\boldsymbol{\alpha}} = \boldsymbol{\alpha}_Q \mathbf{.Q} + (1/2)\mathbf{Q}.\boldsymbol{\alpha}_{QQ}\mathbf{.Q}$. For the backscattering Raman intensity, for example, we get $I_{R,180}(\omega) = \frac{K}{1-\exp(-\omega/kT)} \sum_{\alpha=1..3} \sum_{\beta=1..3} \mathrm{Re}(7\boldsymbol{\alpha}_{R,\alpha\beta}{}^{*}(\omega)\boldsymbol{\alpha}_{R,\alpha\beta}(\omega) + \boldsymbol{\alpha}_{R,\alpha\alpha}(\omega)^{*}\boldsymbol{\alpha}_{R,\beta\beta}(\omega))$. The constant K was chosen to one, as absolute intensities are rarely measured; *k* is the Boltzmann constant and *T* temperature. The exponential factor accounts for scattering from excited vibrational levels as derived in the harmonic limit. Note that the temperature excitations need not to be considered for absorption or VCD in the harmonic limit at all, and they influence is supposedly small also in general.

By replacing the dipole operator by the electric dipole-magnetic dipole polarizability $\hat{\mathbf{G}}' = \mathbf{G}'_Q \mathbf{.Q} + (1/2)\mathbf{Q}.\mathbf{G}'_{QQ}\mathbf{.Q}$ (also referred to as the optical rotation tensor), and the electric dipole-electric quadrupole polarizability $\hat{\mathbf{A}} = \mathbf{A}_Q \mathbf{.Q} + (1/2)\mathbf{Q}.\mathbf{A}_{QQ}\mathbf{.Q}$, we can calculate Raman optical activity. For example, the backscattering incident circular polarized light intensity is equal to

$$\Delta I_{R,180}(\omega) = \frac{8K}{1-\exp(-\omega/kT)} \sum_{\alpha=1..3} \sum_{\beta=1..3} \mathrm{Re}(3\boldsymbol{\alpha}_{R,\alpha\beta}{}^{*}(\omega)\mathbf{G'}_{R,\alpha\beta}(\omega) - \boldsymbol{\alpha}_{R,\alpha\alpha}{}^{*}(\omega)\mathbf{G'}_{R,\alpha\alpha}(\omega) + \sum_{\delta=1..3} \sum_{\gamma=1..3} \varepsilon_{\alpha\gamma\delta}\boldsymbol{\alpha}_{R,\alpha\beta}(\omega)^{*}\mathbf{A}_{R,\gamma\delta\beta}(\omega))$$

.

Chapter 7

Results

7.1 Integration time optimization

First we have investigated the sensitivity of the method to the size of the integration time step. For this we used a water dimer (Fig. 7.1), as a typical simple model used in many theoretical studies. The calculation was done in harmonic oscillator approximation as we were focused on testing the method and not on the exact frequencies of the vibrations. We did a geometry optimalization for water dimer in normal mode coordinates by using Gaussian 03, also we obtained the dipole derivatives according to the first step in Implementation (Chapter 6.3) with a help from program *pmz* programmed by Bouř [20] used for numerical differentiations and generating Gaussian inputs.

A lot of small programs programmed by Bouř helped us in our study. *MCM95* - was used for drawing and imaging of the molecule, initial symmetrization and generation a Gaussian input file; *gar* – to extract force field, atomic polar and axial tensors and polarizability derivatives from Gaussian 03 archive; *gg* – to get geometry from Gaussian output; *new1* – to define internal vibrational and symmetry-adapted vibrational coordinates; *new2* – to define scaling factors and atomic masses for vibrations; *new4* – to calculate vibrational frequencies in Cartesian coordinates; and later on for analysis: *tabprn* - generates XY spectrum from intensities in .TAB files; and *SC95* – as a optical spectra viewer. All these programs can be found on Petr Bouř's webpage [20].

For exact Fourier transformation the peak positions [21] in the ω-spectrum are constant. Previous simulation of the vibrational spectra using classical molecular dynamics trajectories revealed a significant dependence of the Fourier-transformed frequencies on the integration steps [22].

Indeed, as shown in Figure 7.2, where the water dimer bending vibration frequency is plotted as a function of the integration time step for the peak at 1553 cm^{-1} from the absorption spectra of the water dimer. Obviously, larger steps introduce errors of over 100 cm^{-1}, however, for steps below ~ 0.02 fs the frequency stabilizes. Thus we can concur that 0.02 fs is sufficient enough because deviations from the limit $dt \rightarrow 0$ are infinitesimal.

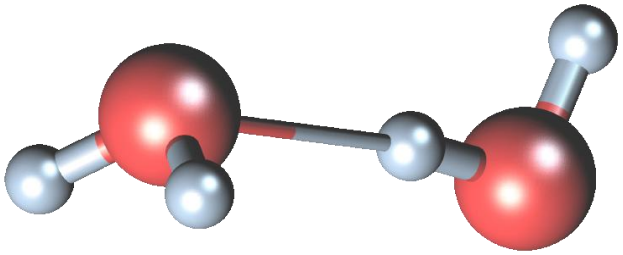

Figure 7.1. *A representation of water dimer, which was used as a simple model in our study. Often called "theoretical Guinea pig"[23]*

This is a relatively small fraction of the period of the corresponding harmonic motion, $T = 2\pi / \omega \approx 21 fs$. Previous studies [22] showed that for harmonic wavefunction propagations, longer integration steps of ~ 0.1 fs could be used. We explain the need to use shorter integration steps for the anharmonic case even for lower-frequency states by a coupling to the higher-frequency states included in the Hamiltonian.

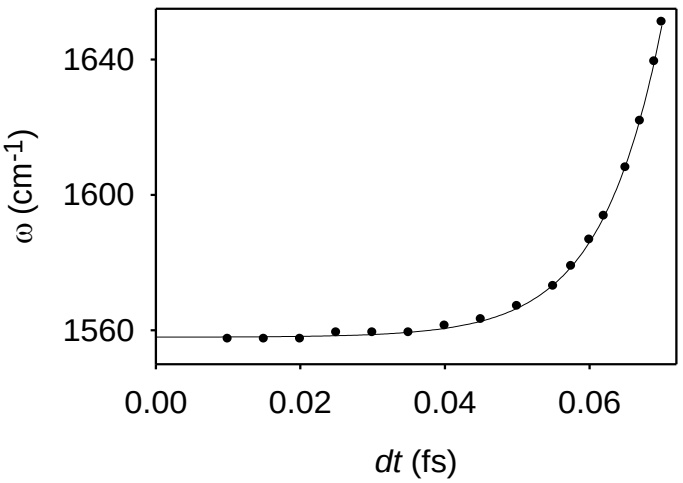

Figure 7.2. *The dependence of the water stretching band frequency on the integration step, for a water dimer.*

7.2 Band Width Convergence

The consequence of the finite interval of time propagation is that spectral peaks are not infinitely sharp but have finite widths. Therefore, it is necessary to establish the number of the time propagation steps needed to obtain sufficiently narrow bands.

The band width is documented in Figure 7.3 for the water dimer, where points are fitted with a function of type t^{-1}. The band width dependence on propagation time was calculated for the water dimer's peak at 1553 cm^{-1} in the absorption spectra. As expected [21], it is inversely proportional to the integration time ($\Delta\omega \sim t^{-1}$). As the width converges relatively slowly, the method does not seem to be usable for high-resolution spectra; in that case many spectral points are additionally needed per frequency interval, which would further slow down the computations. Fortunately, for typical biomolecular spectra inhomogeneous band broadening is quite large, of the order of ~20 cm^{-1}, so that the propagation times can be limited accordingly. That means that for a 0.02 fs time step (used to achieve a high precision of central frequencies, demonstrated in Figure 7.2) about 4000/0.2 = 200000 propagation points are needed.

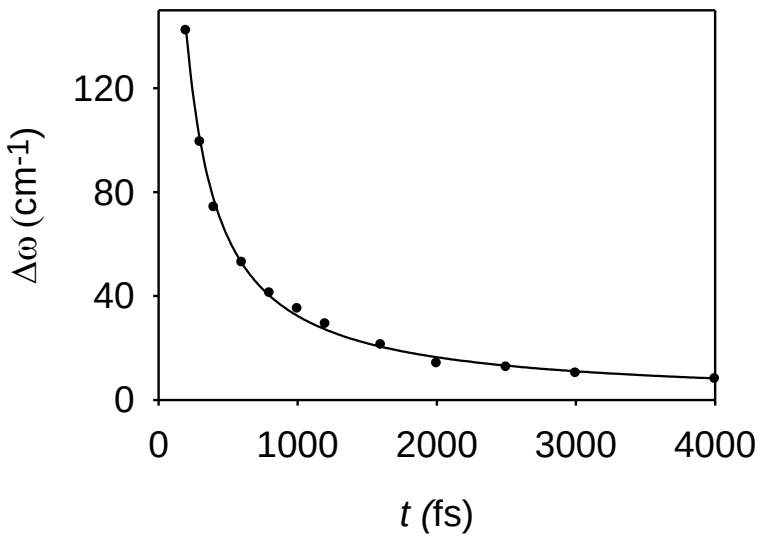

Figure 7.3. *The dependence of the water bending band width on the total integration time for dt=0.02 fs.*

7.3 Trial Vector Averaging

With a sufficiently small integration time step and long enough integration time the procedure yields the correct vibrational frequencies [more discussed in next section and Discussion]. However, the spectral intensities resulting from particular propagation are different as a consequence of the randomly chosen initial vector ψ_R. Thus, to obtain a stable spectrum, which is independent on the choice of the initial conditions, it is necessary to average several runs with random vectors.

For such case we used fenchone because of the more complex spectrum in comparison with water dimer for better illustration of the convergence of the band intensities on the number of the initial vectors ψ_R. The convergence of the Raman band intensities for low and high frequency area of fenchone spectrum are explored in Figure 7.4. For this study we used previously determined parameters for exact spectral frequencies and sufficiently narrow bandwidth, i.e. integration time step 0.02 fs and total integration time 4000 fs.

The resultant Raman spectra are demonstrated for M = 1, 5, 10 and 20 random vectors. While a randomly selected vector (M = 1) provides exact frequencies of the peaks but unrealistic relative intensities, the spectral profile quickly stabilizes. It is obvious that the intensities converge with increasing number of random vectors averaged.

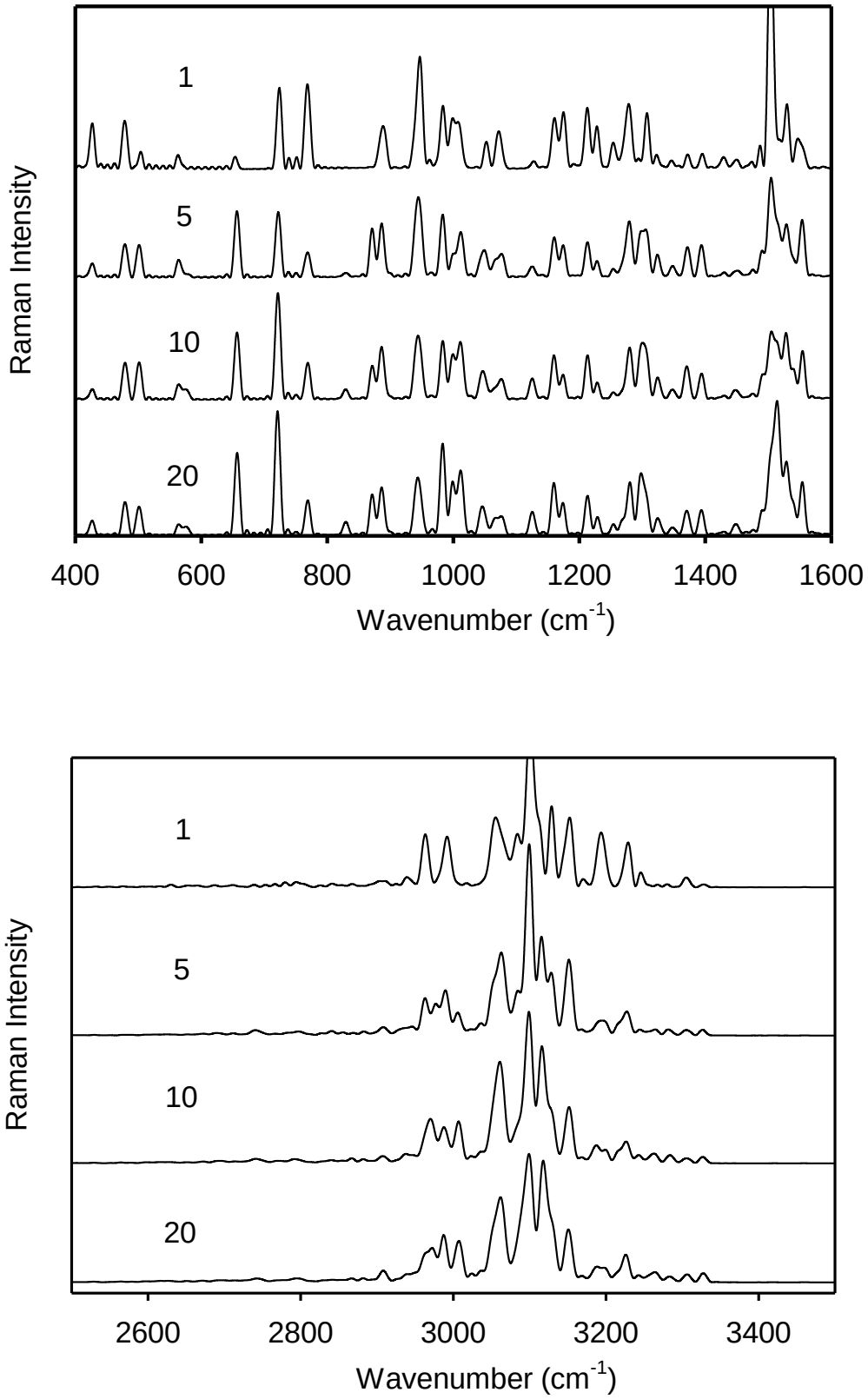

Figure 7.4. *The dependence of the Raman spectra of fenchone on the number of the random vectors used in the propagation (M=1, 5, 10, 20). Top: basic wavenumber range (400 – 1600 cm^{-1})*
Bottom: high wavenumber range (2500 – 3500 cm^{-1})

A better overview how does the intensity distribution depend on vector averaging is in case of ROA spectrum of fenchone. On Figure 7.5 are plotted ROA spectra for a different number of averaged vectors. For this study we used M = 1, 10, 20 and 50. Higher number of averaged vectors was used mainly because we expected more deviation in intensity distribution in comparison with Raman spectra. To compare the intensity distributions we also plotted a spectrum calculated by direct diagonalization method (called exact in Fig. 7.6). For this calculation we used the same propagation step and propagation time as in Figure 7.4.

The dependence on number of vectors averaged is nicely seen for peak at around 1500 cm^{-1} and three peaks around 1300 cm^{-1} in lower frequency area of the spectrum (Figure 7.5 upper plot). It is very interesting that for the low frequency part of the ROA spectra (wavenumber < 1400 cm^{-1}) an average of 20 random vectors is sufficiently enough for good intensity distribution (three peaks at around 1300 cm^{-1}) . But for higher frequencies (wavenumber > 1400 cm^{-1}) additional vectors, in this case 50 vectors, had to be averaged for better intensity distribution. This is clear in case of peak at around 1500 cm^{-1} and peaks in anharmonic part of the spectra, at around 3100 cm^{-1}.

Overall we can conclude that for a higher number of averaged vectors the intensity distribution fit nicely with the exact solution (Direct diagonalization). For a good approximation, 20 averaged vectors are sufficient and more vectors averaged in would generate almost the same spectrum as the Direct diagonalization (Figure 7.5 for M = 50).

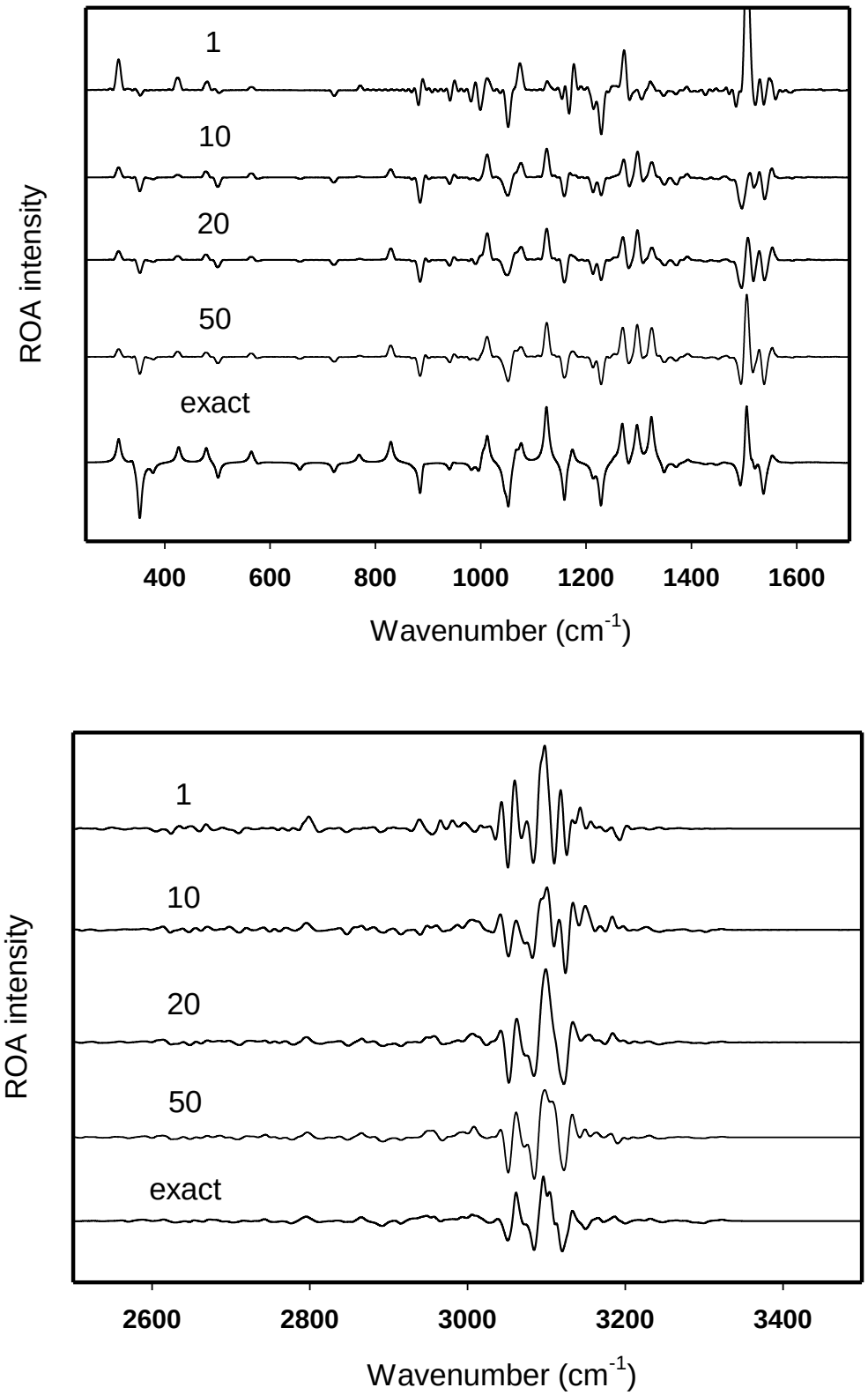

Figure 7.5. *The dependence of the ROA spectra of (1S) fenchone on the number of the random vectors averaged in the propagation (M=1, 5, 10, 20) as compared to the exact result obtained by the direct diagonalization. Top: basic wavenumber range (400 – 1600 cm^{-1}) Bottom: high wavenumber range (2500 – 3500 cm^{-1})*

7.4 Code parallelization

Nowadays most of the calculations are done on several processors, for the sake of speeding up the calculation. In that fashion we wanted to parallelize our code so that the calculation can be done on several processors at ones. The idea is to parallelize the code in such way that the propagation of the system for each randomly chosen vector is done on separate processor. For example, if we want to average our calculation with 20 randomly chosen vectors we can run the calculation on, for example, 10 processors, where every processor would propagate 2 randomly chosen vectors. In that case we would, theoretically, speed up the calculation by 10 times.

Theoretically, that means that the calculation speed is proportional to number of processors used. On Figure 7.6 the dependence of the acceleration on the number of processors used in calculation of fenchone IR spectrum is plotted, where dots represent the dependence and diagonal line represents ideal or theoretical dependence. It is clear from the Figure that the dependence is not linear. This is because of evaluating the system before the propagation takes, in case of fenchone, more time than the propagation itself. Also some programming corrections would help to approach ideal case closer.

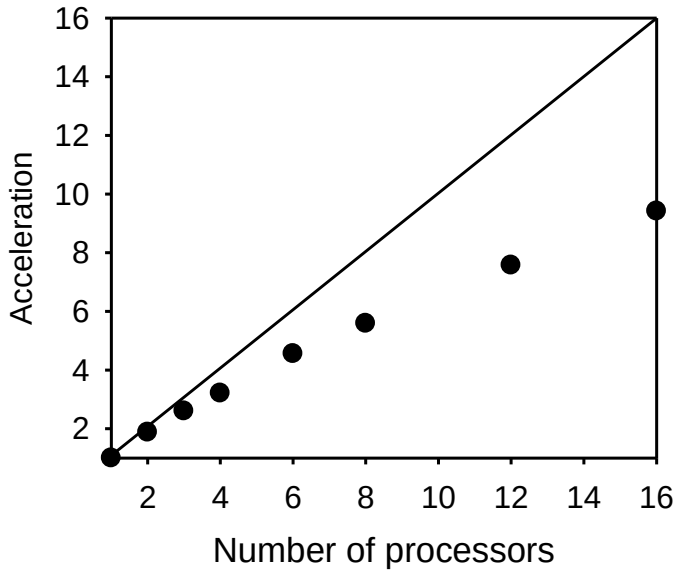

Figure 7.6. *The dependence of the acceleration on the number of processors (done for fenchone IR spectrum calculation, pgf77-OMP-linux software environment, 4 Intel E7330/2.40GHz CPUs on Supermicro X7QCE motherboard)*

7.5 Calculation Time Scaling

Main goal of this study is to show that the FT method becomes faster than Direct diagonalization method and Davidson method for larger Hamiltonian dimensions. This dependence is plotted on Figure 7.7.

Davidson method [4] was developed to solve quantum chemistry problems in which the matrices have diagonal elements that are both large and varying in magnitude. The eigenvalues and vectors are built from the smallest or the largest value iteratively, using a limited number of trial vectors (''Krylov space''). This method is very convenient, for example, for the configuration interaction electron computations, when only a limited number of the low energy electronic states (often just the ground state) is needed. In our FT method we also use iteration (Davidson) method based on the Mitin's modification of the algorithm [24] to calculate ground state of our molecule (see Section 6.3 Implementation). However, for the vibrational problem it is usually not sufficient to find a few largest or smallest eigenvalues, rather a complete spectrum is desired. For such a task Davidson method quickly becomes impractical, as it can be seen from Figure 7.7, where CPU time rapidly prolongs for bigger Hamiltonian dimensions. This prolongation is because each new vector has to be normalized to the rest and with high number of vectors it becomes impractical.

The Householder transformation and the following complete diagonalization routine based on the QR decomposition algorithm provide the fastest in-memory procedure for the determination of the eigenvectors and eigenvalues of a real symmetric matrix [21]. The direct (Householder) method has a N^3 dependence on the Hamiltonian dimension and huge memory requirements for bigger Hamiltonians. This method is also used by Gaussian program package [25].

In Figure 7.7 we can see that the complete Davidson diagonalization is faster than the time propagation up to Hamiltonian dimension of *N~300* and then the time quickly grows to immeasurable values. The direct Householder diagonalization is more efficient up to *N~5000*, which can be somewhat improved by skipping the projection of the zero-vibrational modes (rotations and translations) from the force field. However, because of the N^3 dependence and big memory requirements of the direct diagonalization method, the FT method of the propagation in time becomes the most usable method for larger Hamiltonians (as it can be seen on Figure 7.7). For this

set of FT parameters the condition of the efficiency is for Hamiltonian dimension higher than *5000*. This fact means that the FT method is more convenient for bigger molecules, i.e. proteins, peptides etc. We must mention that this calculation was done with 10000 steps of 0.02 fs propagation time and only for one random vector, as it was just an illustration of the dependence. This means that the actual boundary between efficiency of FT method to direct diagonalization for bigger molecules, as they need more random vectors and greater propagation time, is higher, but still FT method remains faster.

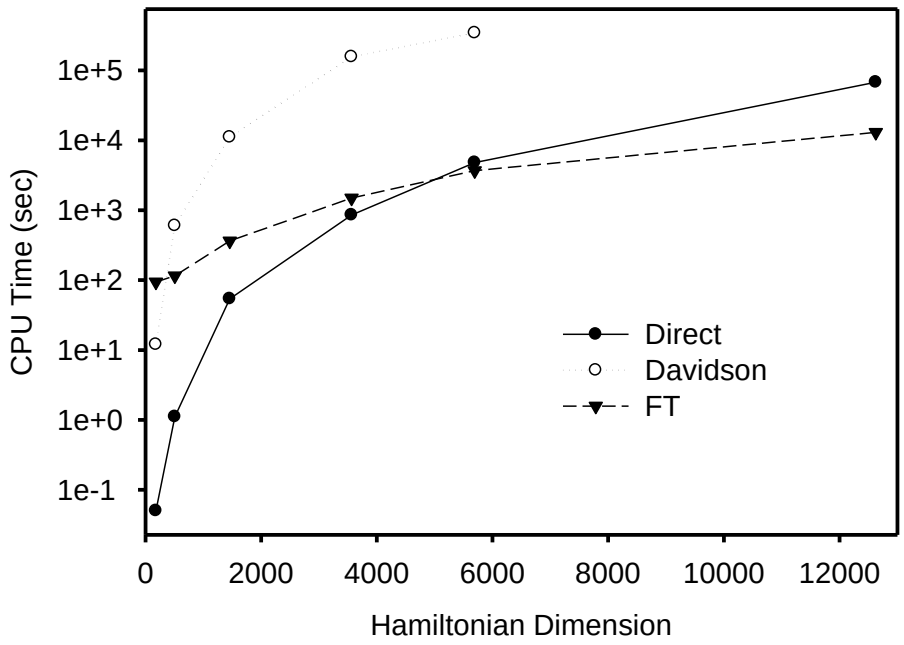

Figure 7.7. *Time needed for the Hamiltonian diagonalization (for the direct and Davidson methods) and for a FT spectral generation, as a function of the Hamiltonian dimension. The Davidson iteration was limited to wavenumbers below 2000 cm*$^{-1}$*, the FT computation was done with 10000 steps and one random vector only.*

7.6 Comparison with Experimental Data

In previous five sections we tested FT method to determine the optimum parameter set for a good simulation of vibrational molecular spectra. In section 7.1 we have shown that in order to have exact frequencies the sufficient integration step is 0.02 fs. In section 7.2 we have determined that for sufficiently narrow peak we must propagate the system for at least 3000 fs, i.e. for a 0.02 fs propagation time step we need 150 000 propagation steps. Finally we have determined that for a proper ratio of intensities we need to average at least over 20 random vectors. Taking this parameter set we calculated the Raman and ROA spectra for (1S)-(+) enantiomer of fenchone.

The comparison with experimental data is given on Figure 7.8. All the calculated frequencies are shifted by 200 cm^{-1}, so that the first peak at 600 cm^{-1} suits the experimental data. This not a good correction from a theoretical point of view, but it is a normal procedure in nowadays calculations of spectra. More about this subject is discussed in chapter Discussion. The size of the Hamiltonian matrix is determined by states considered, in this case 49584 states. Total time of the calculation was 8 days, 17 hours and 49 minutes.

Generally, calculated spectra predicted the shape of the spectra and the ratio of the intensities with great efficiency, especially in lower frequency area (harmonic part) of the spectra, i.e. for frequencies from 0 to approximately 2000 cm^{-1}. The shape of the spectra satisfies the experimental data even for higher frequencies. This is nicely seen on ROA spectrum where signs of the peaks suit the experimental data. Nevertheless, predicted frequencies in higher frequency area (anharmonic part) of the spectra don't satisfy the experimental data. The reason for this is obviously use of sufficiently not good enough potential. Even though we used harmonic approximation (see Section 3.2) with VCI (see Section 4.3) with a $\eta = 0.002$ ratio from Eq. 4.14, the spectra did not have precise frequencies in anharmonic part of the spectra. VCI correction is a mandatory thing in vibrational calculations mainly for sake of time of the spectrum calculation. We used this correction in other calculations, as well, also with the same η ratio. We also added an option from program S4 [20] called NQ1, which determines how many modes can be excited for a basis state, in this case we allowed only 3 states to be excited. But this option did not bring us a significant improvement.

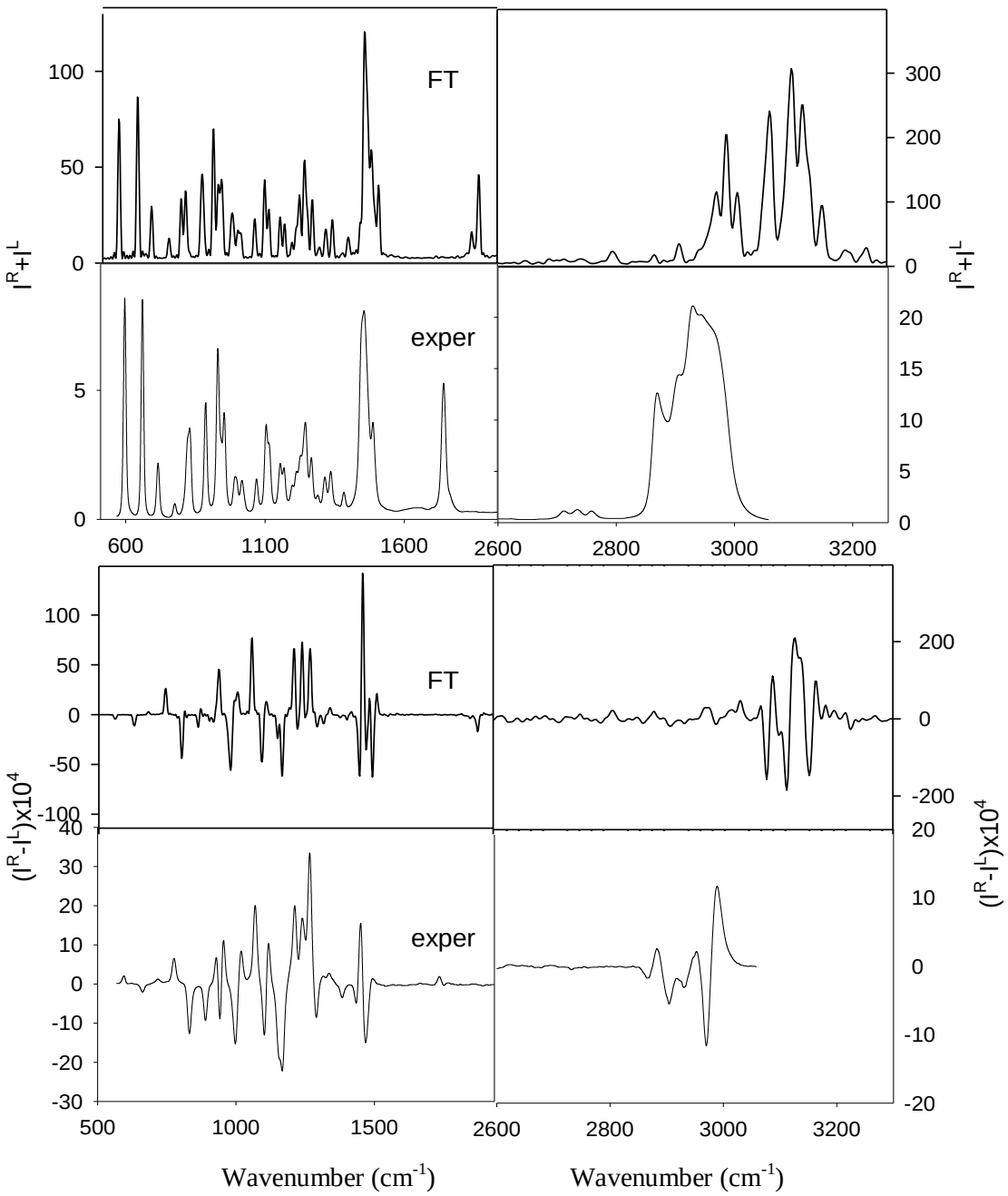

Figure 7.8. *Comparison of the calculated Raman (top) and ROA (bottom) spectra using FT method with experimental data for (1S)-(+) fenchone. (Calculation was done in harmonic approximation with 150000 steps of 0.02 fs propagation steps and averaged with 20 random vectors). Experimental data were taken from diploma thesis of M. Kubáňová [29].*

Having this in mind, our next step was to implement other anharmonic corrections, i.e VSCF and PT2 (see Chapter 4), to vibrational potential in order to calculate more precise spectrum. Also we wanted to see if the combination of the three methods would generate the closest spectra to the exact solution or if other would be better.

First additional anharmonic treatment to VCI we used in previous calculations was PT2 method (explained in Chapter 4.1) into our calculation of Raman and ROA spectra of (1S)-(+) fenchone. PT2 is implemented in S4 program in three ways. Normal PT2 calculation to molecular potential without corrections to degenerated states is calculated automatically if it is not switch off in S4.OPT file with option NOENA. Degenerations corrected PT2, where energies are calculated using Eq. 4.13, is switched on by using option ENA2. A deviation of this method, where only states that have big corrections, i.e. bigger that given limit, are considered, is also implemented in program S4 by using option ENAS. The limit, for which are the certain states left out from PT2 correction, is regulated by option ASL. This certainly speeds up the computational time of the PT2 correction.

For our calculation we used option ENAS with ASL limit of 10 cm^{-1}. Figure 7.9 shows the results from this calculation in comparison with the experimental data for Raman (upper spectra) and ROA (lower spectra). For this study we used 150000 steps of 0.02 fs propagation step. It was then averaged with 20 random vectors. Procedure works in such way that firstly calculates perturbation to the molecular potential [Eq. 3.12] and then uses this potential for a time propagation of the system. Total time of this calculation was 6 days, 10 hours and 13 minutes. The Hamiltonian had the same size as in previous calculation, i.e. 49584 states.

Just as in previous figure 7.8, also in this figure all the calculated frequencies are shifted, so that the first peak at 600 cm^{-1} suits the experimental data. Exception is that in this case the shift in wavenumber is 150 cm^{-1}. This is the first significant improvement in comparison to previously calculation without PT2 correction [Figure 7.8]. Also the peak in high anharmonic part (experimentally around 2950 cm^{-1}) shifted to lower frequencies, i.e. around 3000 cm^{-1}, as well as the peak at 1750 cm^{-1} (experimental data) shifted to lower frequencies (around 1850 cm^{-1}).

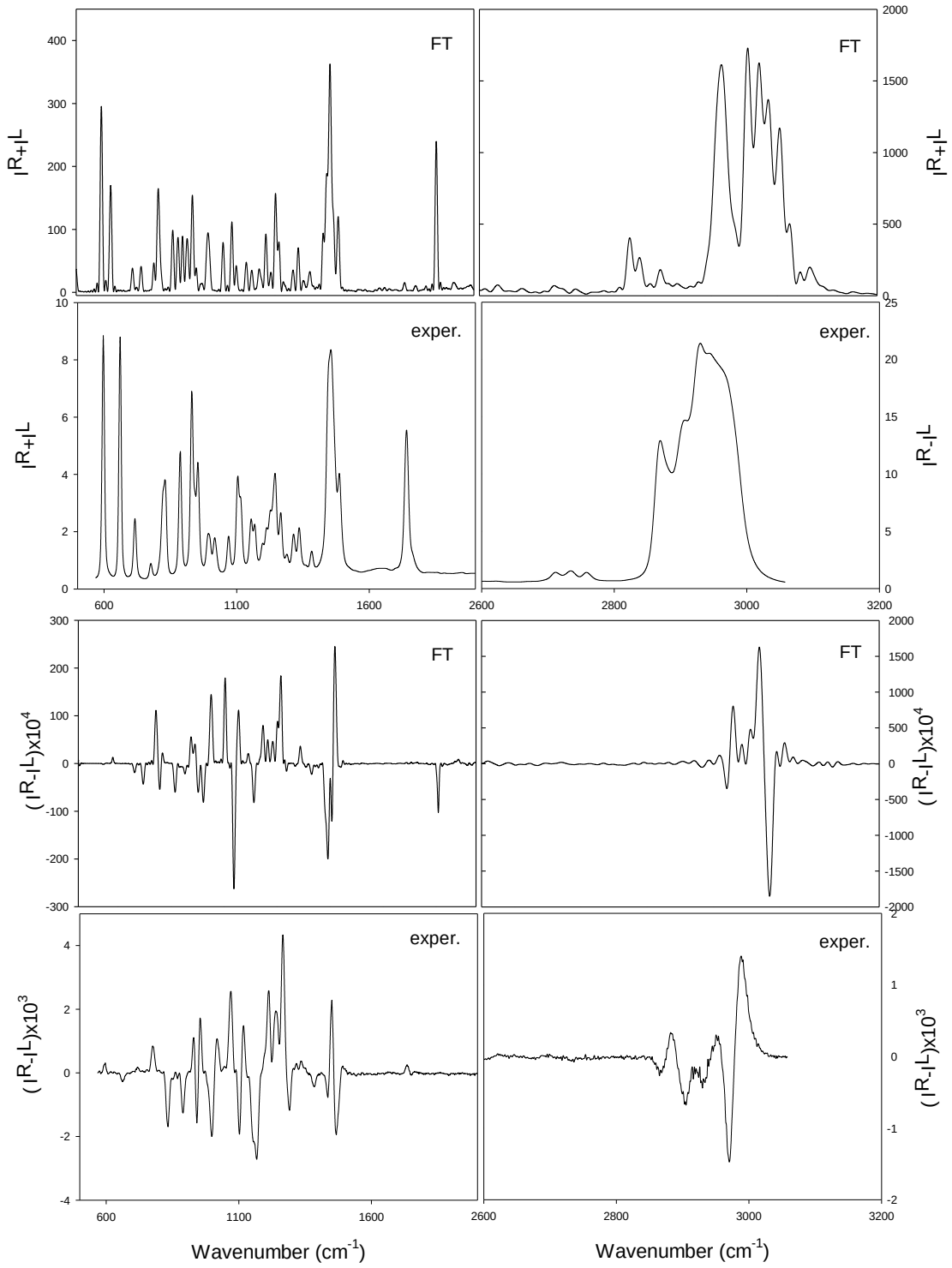

Figure 7.9. *Comparison of the experimental data for (1S)-(+) fenchone with calculated Raman (top) and ROA (bottom) spectra using FT method with VCI and PT2 corrections (Calculation was done with 150000 steps of 0.02 fs propagation steps and averaged with 20 random vectors, using method ENAS with ASL limit of 10 cm^{-1}). Experimental data were taken from diploma thesis of M. Kubáňová [29].*

Beside the improvements in the position of the anharmonic peaks in Raman spectrum, the ROA spectrum suffered in terms of spectral shape. The calculated spectrum somehow less coincides with experimental data, mainly the peak at 1500 cm^{-1} and strong peak in anharmonic part. Paradoxically they got the reversed signs in comparison with previous calculations, where the signs of the peaks were calculated correctly.

Next additional method to harmonic approximation was VSCF (Chapter 4.2). This method is implemented into S4 program through option VSCF. Just as theory states, the molecular potential is a sum of individual oscillators (atoms), as in Eq. 4.7, and the energies from each oscillator is obtained by solving the Schrödinger equation for each oscillator (Eq. 4.9) self-consistently until all energies stabilize. In that way program S4 first calculates VSCF energies and then builds the vibrational potential *V* before it starts propagating system in time.

Resulting Raman and ROA spectra in comparison with experimental data are shown on Figure. 7.10. Total time of this calculation was 7 days, 11 hours and 42 minutes. Also in this case we used shift of wavenumber, so that the first peak at 600 cm^{-1} suits the experimental data. For these resultant spectra the shift was also 150 cm^{-1}. Also the propagation time, time step and number of random vectors are the same as for previous calculation. As in previously calculated spectra, the shape of the Raman spectrum exhibits good correspondence with experimental spectrum. The only problem is the positions of the peak at 1750 cm^{-1}, which is in this case (1800 cm^{-1}) better in comparison with calculation with PT2 correction (1850 cm^{-1}), and the band in anharmonic area. The bad correspondence of calculated ROA spectrum with experimental data is still present, exact that in this case the shape of spectrum better coincides with experimental data. Still, the band in high frequency area has the reversed signs and unsatisfying shape.

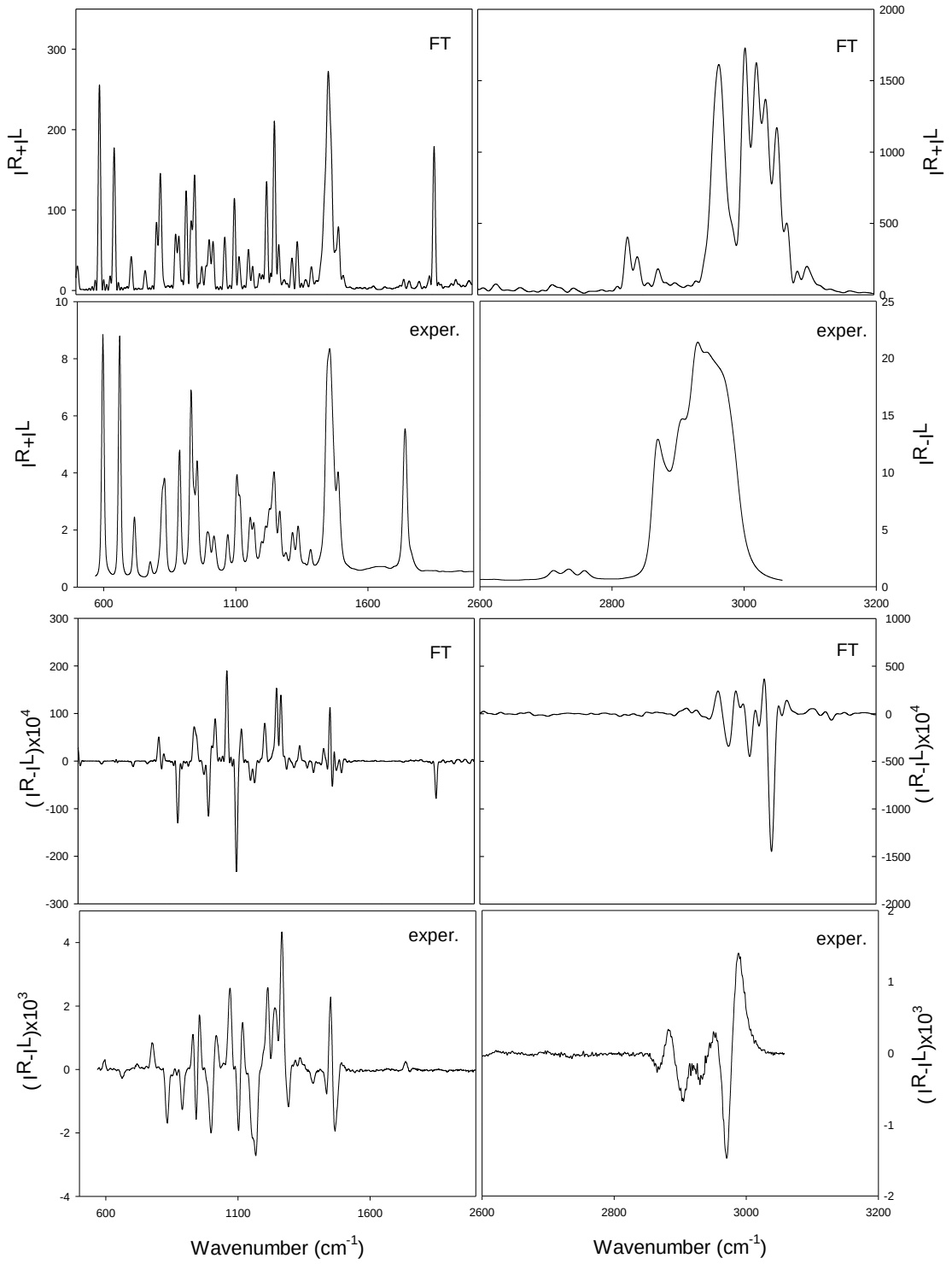

Figure 7.10. *Comparison of the experimental data for (1S)-(+) fenchone with calculated Raman (top) and ROA (bottom) spectra using FT method with VCI and VSCF corrections. (Calculation was done with 150000 steps of 0.02 fs propagation steps and averaged with 20 random vectors). Experimental data were taken from diploma thesis of M. Kubáňová [29].*

Lastly, we wanted to combine all of the anharmonic corrections (Chapter 4) with FT method to see if it will somehow improve the calculations. So, in this case we turn both VSCF and ENAS options in S4 program. One difference from previous calculation with PT2 correction is that we used ASL limit of 20 cm^{-1} for the sake of time of the calculation. All the other options such as propagation time, time step and number of random vectors remained the same. Also the η ratio for VCI remained the same as in previous calculations.

Results are plotted on Figure 7.11. As expected the total time for this calculation was the longest and it took 11 days, 10 hours and 32 minutes. First the program calculated the PT2 corrections and then it did VSCF calculation. Main difference from previously calculated spectra is the shift in wavenumber. In this case we shifted wavenumber scale only for 50 cm^{-1}. It is also very interesting that the peaks are narrower than in previous results. Besides that, the calculated Raman spectrum has very good correspondence with experimental data, even in the high frequency area, where the band approaches exact frequency of the one from experimental data. Only imperfection is the peak in 1800 cm^{-1}, which does not seem to moved in comparison with previous results. Worst it is for ROA spectrum, where we somehow seem to have lost the three peaks at around 1250 cm^{-1}. Also a big negative peak at around 1500 cm^{-1} appeared which does not have any experimental basis. On contrary to this, the anharmonic band in this case has the correct signs and is not so far from experimental one in terms of the shape.

Methods	**Wavenumber shift [cm^{-1}]**	**Calculation time [min]**
VCI	200	12589
PT2,VCI	150	9253
VSCF,VCI	150	10782
VSCF,PT2,VCI	50	16472

Table 7.1. *Values of wavenumber shift and calculation time for four types of combination of methods used for calculation of Raman and ROA spectra of (1S)-(+) fenchone. Calculations were done on one processor with 150000 steps of 0.02 fs propagation steps and averaged with 20 random vectors.*

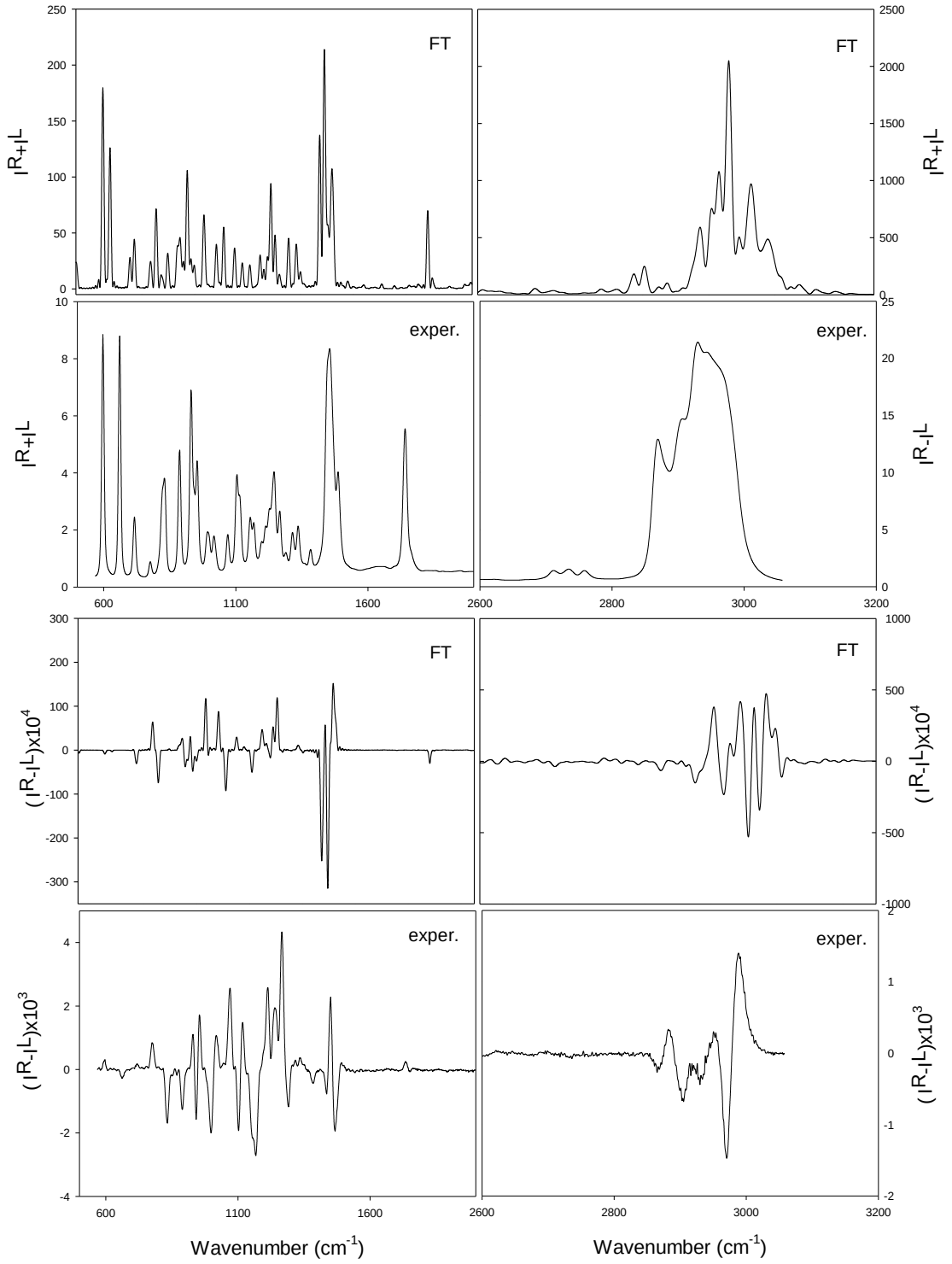

Figure 7.11. *Comparison of the experimental data for (1S)-(+) fenchone with calculated Raman (top) and ROA (bottom) spectra using FT method with VCI, PT2 and VSCF corrections. (Calculation was done with 150000 steps of 0.02 fs propagation steps and averaged with 20 random vectors, using method ENAS with ASL limit of 20 cm^{-1}). Experimental data were taken from diploma thesis of M. Kubáňová [29].*

Discussion and Conclusions

In this work we explored a new method for generating vibrational spectra by propagating trial wavefunction in time and Fourier transforming it to get the frequency spectra. First, we introduced the theory of molecular vibrational analysis, anharmonic corrections to the harmonic approximation, and basic Raman and ROA theories. Then we demonstrated the Prague ROA spectrometer and showed the data that were measured for the fenchone compound. The spectra are plotted in Figure 5.8 and as it was mentioned above, this data cannot be used for theoretical comparison as they are only measured in harmonic part of vibrations, i.e. < 2000 cm^{-1}. For that reason, the data used for theoretical comparison were measured by M. Kubáňová and published in her diploma thesis in 2009.

Afterwards we presented the theory of FT method, how is it implemented into S4 program [20], and the modifications of the algorithm for calculation of IR, VCD, Raman and ROA spectra. Then we tested our method in terms of propagation time optimalization, band width convergence and trial vector averaging. Fig. (7.2) shows the effect of peak positioning on propagation time step value. From this we determined the appropriate time step of propagation (0.02 fs). Fig. (7.3) demonstrates the dependence of total time propagation on band width, from which we concluded that the total time of more than 3000 fs is needed for a sufficiently narrow band width. As it was mentioned above, the method does not seem to be usable for high-resolution spectra. For this case we would need many spectral points per frequency interval, which would further slow down the computations. Fig. (7.4) and (7.5) show the dependence on number of random vectors used in averaging for Raman (Fig. 7.4) and ROA (Fig. 7.5) spectra. From this we concluded that sufficient amount of vectors averaged for Raman spectrum is 20 and for ROA is about 20. Generally, 20 random vectors averaged is sufficient for higher part of the spectrum (i.e. > 2000 cm^{-1}), but more vectors are needed for lower frequency range.

After that we test more technical details of the method, as the dependence on number of processors for code parallelization (Fig. 7.6) and comparing the total time fo the calculation with other methods (Fig. 7.7). As it is clear from Fig. (7.6), the code parallelization is not ideal, but sufficient for most cases. Fig. (7.7) is probably the most pleasant characteristic of the FT method, as it shows how the method becomes efficient in CPU time for big Hamiltonian dimensions in comparison with Direct

diagonalization (most common method that is used by Gaussian program pack [25]) and Davidson method [4]. This means that for large systems such as proteins, the FT method is the fastest one and also accurate as the others; Fig. (7.5) shows the comparison with spectrum obtained by the Direct diagonalization.

Then we wanted to compare the data with experiment. We must also point out that all the previous calculations were done in harmonic approximation, as we were focused mainly on characteristics of the method and not the exact frequencies of the vibrations. When we tried to compare calculated spectra with experimental data we came to conclusion that some corrections have to be done. First we added VCI (Chapter 4.3) correction with appropriate $\eta = 0.002$ ratio from Eq. (4.14) and also when that was not enough, we added an option from program S4, called NQ1. Figure 7.8 compares calculated spectra for harmonic approximation with above mentioned corrections. Also we have shifted the spectrum in wavenumber by 200 cm^{-1} in order to do a sort of a "calibration". The used anharmonic approximation approximates well low states (< 2000 cm^{-1}), but shifts higher states towards higher energies so that calculated difference is greater than the actual one. It is clear that by using other anharmonic corrections (PT2 and VSCF) the frequencies shift to lower values and we only used 150 cm^{-1} for VCI + PT2 (Fig. 7.9) and VCI + VSCF (Fig. 7.10) and only 50 cm^{-1} for the combination of all three anharmonic corrections (Fig. 7.11). Even though these corrections improved frequency positions; we lost the good match in shape of the ROA spectrum as it is shown in for Fig. (7.8). Besides, for VCI + PT2 the calculated band profile in anharmonic part of the ROA spectrum had the reverse signs. Improvement came with VSCF and for the combination of all three methods (Fig. 7.11) the band has almost the exact frequency and relative intensities. Just as mentioned above, for a better relative intensity in this part of the spectra, we would need to average over more random vectors in order to have better intensities of the peaks in high frequency band. Also in future studies of fenchone compound, it would be better to use smaller propagation time, as the peaks in Fig. (7.11) are narrower than the experimental ones. Also adding NQ1 option in calculation would improve the spectrum, as most of the experimental data are measured for the specimen that is mostly in ground state. This can increase the time of the calculation as the total time of that calculation (Fig. 7.8) was 8 days, 17 hours and 49 minutes. It was still greater than for the VCI + PT2 and VCI + VSCF, which took 6 days, 10 hours and 13 minutes, resp. 7 days, 11 hours and 42 minutes. As expected the total time for the calculation

with all three anharmonic corrections was the longest and it took 11 days, 10 hours and 32 minutes. Comparison of both calculation time and wavenumber shift for different methods, is shown on Table 7.1.

In future studies it would be good to look at larger systems with much higher number of atoms and to compare the calculation time with the calculation times from other methods, mainly with the direct diagonalization. In this way, we can implement all the corrections needed while not increasing total calculation time. From Fig. (7.7), we see that the FT method becomes the most efficient one for large systems, i.e. for approximately more than 1000 atoms.

Bibliography

[1] Kapitán J.; Baumruk, V.; Kopecky Jr.; Pohl, R.; Bouř, P. *J. Am. Chem. Soc.* **2006**, *128*, 13451.

[2] Narayanan, U.; Keiderling, T. A. *J. Am. Chem. Soc.* **1983**, *105*, 6406.

[3] Pulay, P. *J. Phys. Chem.* **1995**, *99*, 3093-3100.

[4] Davidson, E. R. *J. Comput. Phys.*, **1975**, *17*, 87.

[5] Papoušek, D.; Aliev, M. R. *Molecular Vibrational/Rotational Spectra*; Academia: Prague, **1982.**

[6] Daněček, P.; Bouř, P. *J Comp Chem*, **2007**, *28*, 10.

[7] Daněček, P.; Kapitan, J.; Baumruk, V.; Bednarova, L.; Kopecky, V.; Bouř, P. *J. Chem. Phys.* **2007**, 126, Art. No. 224513.

[8] Fujisaki, H.; Yagi, K.; Hirao, K.; Straub, J. *Chem. Phys.Lett.* **2007**, *443*, 6.

[9] Bowman, J. M. *J. Chem. Phys.* **1978**, *68*, 608.

[10] Califano, S. *Vibrational states*, Wiley, London, **1976.**

[11] Skála, L. *Základy kvantové chemie*, Karolinum, Praha, **1994**.

[12] Davidov A. S.: Kvantová mechanika, SPN, **1978**.

[13] Demtröder, W. *Atoms, Molecules and Photons*, Springer, Berlin, **2006**.

[14] Matsunaga, N; Chaban, G. M.; Gerber, R. B. *J Chem Phys*, **2002**, *117*, 3541.

[15] Carter S.; Bowman J. M.; Handy N. C. *Theor. Chem. Acc.* **1998**, *100*, 191.

[16] Møller, C.; Plesset, M. S. *Phys. Rev* **1934**, *34*, 618.

[17] Brauer, B.; Chaban, G. M.; Gerber, R. B. *Phys Chem Chem Phys* **2004**, *6*, 2543.

[18] de.wikipedia.org/wiki/fenchone

[19] Ivani, I.; Baumruk, V.; Bouř, P. *J. Chem. Theory & Comput.* ***(submitted)***.

[20] Bouř, P. *Program S4*, Academy of Sciences: Prague, **1994-2010.**

[21] Press, W. H.; Teukolsky, S. A.; Vetteling, W. T.; Flannery, B. P. *Numerical Recipes in Fortran*, 2nd ed.; Cambridge University Press: New York, **1992**.

[22] Horníček, J.; Kaprálová, P.; Bouř, P *J. Chem. Phys.* **2007**, *127*, Art. No. 084502.

[23] en.wikipedia.org/wiki/Water_dimer

[24] Kubelka, J.; Keiderling, T. A. *J. Am. Chem. Soc.* **2001**, *123*, 6142.

[25] Frisch, M. J.; Trucks, G. W.; Schlegel, H. B.; Scuseria, G. E.; Robb, M. A.; Cheeseman, J. R.; Montgomery, Jr., J. A.; Vreven, T.; Kudin, K. N.; Burant, J. C.; Millam, J. M.; Iyengar, S. S.; Tomasi, J.; Barone, V.; Mennucci, B.; Cossi, M.; Scalmani, G.; Rega, N.; Petersson, G. A.; Nakatsuji, H.; Hada, M.; Ehara, M.; Toyota, K.; Fukuda, R.; Hasegawa, J.; Ishida, M.; Nakajima, T.; Honda, Y.; Kitao, O.; Nakai, H.; Klene, M.; Li, X.; Knox, J. E.; Hratchian, H. P.; Cross, J. B.; Bakken, V.; Adamo, C.; Jaramillo, J.; Gomperts, R.; Stratmann, R. E.; Yazyev, O.; Austin, A. J.; Cammi, R.; Pomelli, C.; Ochterski, J. W.; Ayala, P. Y.; Morokuma, K.; Voth, G. A.; Salvador, P.; Dannenberg, J. J.; Zakrzewski, V. G.; Dapprich, S.; Daniels, A. D.; Strain, M. C.; Farkas, O.; Malick, D. K.; Rabuck, A. D.; Raghavachari, K.; Foresman, J. B.; Ortiz, J. V.; Cui, Q.; Baboul, A. G.; Clifford, S.; Cioslowski, J.; Stefanov, B. B.; Liu, G.; Liashenko, A.; Piskorz, P.; Komaromi, I.; Martin, R. L.; Fox, D. J.; Keith, T.; Al-Laham, M. A.; Peng, C. Y.; Nanayakkara, A.; Challacombe, M.; Gill, P. M. W.; Johnson, B.; Chen, W.; Wong, M. W.; Gonzalez, C.; and Pople, J. A.; Gaussian, Inc., Wallingford CT, **2004**.

[26] Barron, L. D.; Bogaard, M. P.; Buckingham, A. D. *J. Am. Chem. Soc.* **1973**, *95*, 603.

[27] Barron, L. D. *Molecular Light Scattering and Optical Activity*, 2nd edition, Cambridge University Press, Cambridge, **2004**.

[28] Kapitán, J. *Doctoral thesis*, MFF UK, Praha, **2006.**

[29] Kubáňová M. *Diploma thesis*, MFF UK, Praha, **2009**.